OPTOELECTRONIC CHARACTERIZATION OF ORGANIC PHOTODIODES, LIGHT SOURCES AND PHOTOLUMINESCENT EMITTERS

A Thesis

Submitted in partial fulfillment for the degree of

MASTER OF SCIENCE

(Materials Science)

By

ANARANYA GHORAI

CHEMISTRY AND PHYSICS OF MATERIALS UNIT

JAWAHARLAL NEHRU CENTRE FOR ADVANCED SCIENTIFIC RESEARCH

(A DEEMED UNIVERSITY)

Bangalore – 560064

Dedicated to my grandparents

Declaration

I hereby declare that the matter embodied in the thesis entitled *"**OPTOELECTRONIC CHARACTERIZATION OF ORGANIC PHOTODIODES, LIGHT SOURCES AND PHOTOLUMINESCENT EMITTERS**"* is the result of the work carried out by me under the supervision of Prof. K. S. Narayan, at Molecular Electronics Laboratory, in Chemistry and Physics of Materials Unit, Jawaharlal Nehru Centre for Advanced Scientific Research, Bangalore, India. It has not been submitted for the award of any degree or diploma or associateship of any other university or institute.

In keeping with the general practice in reporting scientific observations, due acknowledgement has been made whenever the work described is based on the findings of other investigators.

(Anaranya Ghorai)

JAWAHARLAL NEHRU CENTRE FOR ADVANCED SCIENTIFIC RESEARCH

Bangalore – 560064

K. S. NARAYAN
Professor
Dean (Research and Development)
Phone: +91 80 2208 2822/2548
E-mail: narayan@jncasr.ac.in
Fax: + 91 80 2208 2766

March 31st, 2017

Certificate

I hereby certify that the matter embodied in this thesis entitled *"**OPTOELECTRONIC CHARACTERIZATION OF ORGANIC PHOTODIODES, LIGHT SOURCES AND PHOTOLUMINESCENT EMITTERS**"* is the result of the work carried out by Mr. Anaranya Ghorai at the Molecular Electronics Laboratory, in Chemistry and Physics of Materials Unit, Jawaharlal Nehru Centre for Advanced Scientific Research, Bangalore, India, under my supervision and it has not been submitted for the award of any degree or diploma or associateship of any other university or institute.

Prof. K. S. Narayan

(Research supervisor)

Acknowledgements

I would like to express my sincere thanks to my research supervisor Prof. K. S. Narayan, for suggesting me this problem. His guidance and constant motivation have given me confidence in exploring the field.

I thank Prof. C.N.R. Rao for being a constant source of inspiration. The commitment Prof. Rao shows to science is contagious.

I am thankful to my past and present lab-mates, Dr. Ravichandran Shivanna, Dr. Rahul Kumar Sharma, Dr. Suman Banerjee, Prashant, Ashar, Swathi, Raaghesh, Apoorva, Ganesh, Deepak, Nisha, Sumukh, Sukanya and Abdul Aziz for their valuable discussions and their insights have helped me understand better. They have made working in lab interesting and worthwhile.

I want to thank my batchmates Raktim, Pavitra, Anirudh, Srimayee, Ekashmi and Shikha. I also want thank my close friends Monoj, Debdipto, Arkamita, Koushik, Dibyojyoti, Sudip, Arindam, and Sujoy for standing by me through my best and worst times. I thank my other friends and seniors at JNC, Rajiv, Satya, Manodeep Subhajit, Manisha, Abhiroop, Sudeshna, Niloyendu and Satyajit . I thank all my other friends, Integrated PhD family and well-wishers.

Deepest gratitude is due to Prof. N. Chandrabhas, Chairman of Chemistry and Physics of Materials Unit and also our Integrated Ph.D coordinator, for being the best person I know in JNC. I wish I could carry the advices you have given me all my life. I thank my course instructors at JNC, Prof. S Balasubramanium, Prof. Chandrabhas Narayana, Dr. Eswaramoorthy, Dr. Rajesh Ganapathy, Prof. S.M. Shivaprasad, Dr. N.S.Vidhyadhiraja, Prof. Umesh Waghmare, Prof. Subir Das, Prof. Arindam Ghosh, Prof. Ambarish Ghosh, Prof. A.K. Sood, Prof Manoj Verma, Prof. Srikanth Sashtry, Dr. Ranjan Dutta and Prof. Aloknath Chakroborthy for their discussions and lectures.

I also thank my all-time best friends from college Joydeep, Dulak, Aritra, Subhro, Sanglap and Tanmoy for making my life wonderful.

I owe a lot to my teachers especially Dr. Amitava Sil, Dr. Ruma Sengupta, Dr. Pintu Mandal, Dr. Sumanta Mukhyopadhyay, Dr Sabyasachi Mahapatra.

I also thank working staff at JNC and hostel for making life pleasant and easier. Special thanks to Mr Rajkumar from workshop for helping me set up the Faraday cage.

I pay my sincere respect and gratitude to my parents and grandparents without whom I would have succeeded nothing in my life. I thank my father for being a role model to me and inspiring me always and my mother for showering me with love and affection. I thank my brother for being a true friend to me and for being the coolest person I know. I also want to tehnk my grandfather and my late grandmother for making filling my childhood with lot of good memories and motivating me to become a better person.

Preface

The thesis focusses mainly on the fabrication of organic photodiodes to be used as potential detectors for visible light communication

Organic photovoltaic technology is a very promising and cost-effective alternative to other solar energy because of their vast array of advantages such as band gap tunability, high absorption coefficient, low cost, ease of fabrication, etc. Organic photodiodes have the potential to meet the present and future needs of photodiodes because they have matched and sometimes outperformed their inorganic counterparts Chapter 1 gives a brief introduction to optical wireless communication with a small focus on the modulation techniques. The figures of merit for the photodiodes such as the responsivity, temporal response (or optical bandwidth) and dynamic range are discussed in detail in this chapter. A brief introduction of organic semiconductors are described followed by the working of the photodiode

Chapter 2 deals with the fabrication protocols and characterization of a binary blend bulk heterojunction (BHJ) based organic photodiode consisting of poly(9,9-dioctylfluorenyl-2,7-diyl) (PFO) as the donor and [6-6]phenyl-C61-butyric acid methylester (PCBM) as the acceptor.

To enhance the temporal response and responsivity in the near infra-red (NIR) region a NIR dye was added to this binary blend which is discussed in Chapter 3. Apart from PFO, a squaraine derivative with a very narrow absorption range in the NIR region was used to fabricate the OPD. The fabrication protocols and characterization of the ternary blend OPD are focused in the chapter.

Chapter 4 deals with the influence of various photo-luminescent coatings on the wall in the non-line of sight visible light communication. The concepts which utilize the non-line of sight fraction of light incident on a detector assembly in a visible-light communication (VLC) system is introduced and discussed in this chapter. In addition to ambient light, realistic enclosures where VLC is implemented consist of a sizable fraction of scattered and reflected light. The results of VLC systems with detectors responding to contributions from the light source scattered off a surface embedded with fluorescent and phosphorescent emitters besides the direct line of sight signal are presented. Contribution from the emitters takes a form of

discernible fluctuations in the detector signal. The implication of these results from noise analysis of these fluctuations indicates the possibility of utilizing smart coatings to further tailor VLC capabilities. The phosphorescent material used in this paper is Zinc Sulfide (ZnS) which has a lifetime of ~ 3 s. A direct example of energy harvesting is demonstrated where the Li-Fi signal communication persists after switching off the LED source, due to the persistence of phosphor glow for a sufficient duration (~ few hours).

Contents

CHAPTER 1

INTRODUCTION

In the early 19th century, it was discovered that there are some materials which show a decrease in resistance with an increase in temperature[1]. These materials were termed as semiconductors. The first solid state Germanium transistor was demonstrated by Bell labs in 1947[2]. The use of transistors for storing data and to be used as micro-processors became a large focus from the scientific and industrial community. With the invention of light emitting diodes (LEDs), laser diodes and photodiodes, the possibility of optical data communication was realized[3].

In the last four decades, organic semiconductors have brought a revolution in the field of plastic electronics. They have a vast array of advantages such as band gap tunability, high absorption coefficient, low-cost, low-temperature processability, etc. Large academic and industrial efforts have been devoted to fabricate efficient organic LEDs (OLEDs)[4,5], organic photovoltaics (OPVs)[6,7] and organic field effect transistors(OFETs)[8]. Wireless optical communication also called visible light communication (VLC) utilizes off-the-shelf light-emitting diodes (LEDs) and laser diodes as transmitters and detectors to realize fully networked wireless systems. Research in VLC is focused on improving the response speed of LED and photodiode by fabricating LEDs and photodiodes with higher switching speeds or by using better modulation schemes for LEDs and better equalization techniques for photodiodes. *This thesis focusses mainly on the fabrication of organic photodiodes to be used as detectors that can serve as potential candidates for optical communication.*

Section 1.1 gives a brief introduction to optical wireless communication with a small section on the modulation techniques used in LEDs. The figures of merit of commercial photodiodes are focused in Section 1.2. Section 1.3 talks about the basics of organic semiconductors followed by a brief working principle of organic photodiodes in section 1.4.

.

1.1 Optical Wireless Communication

In the last century, wireless communication has been the fastest growing segment of the communications industry. In 1864 James Clerk Maxwell showed mathematically that electromagnetic waves could propagate through free space. However, the existence of electromagnetic waves was experimentally demonstrated by Heinrich Rudolph Hertz in 1888. It was in 1895, Sir Jagadish Chandra Bose demonstrated the first wireless communication using electromagnetic waves to ring a bell remotely by using gunpowder[9]. Since then, wireless communication technology has had many major pathbreaking developments starting from the invention of telegraphy and radio to the invention cellular mobile technology. Wireless technology systems have experienced exponential growth over the last decade and there are currently around two billion users worldwide. Due to this, the available radio spectrum below 10 GHz has become insufficient to all the users worldwide. This has sparked a need for the use of the radio spectrum above 10 GHz[10].

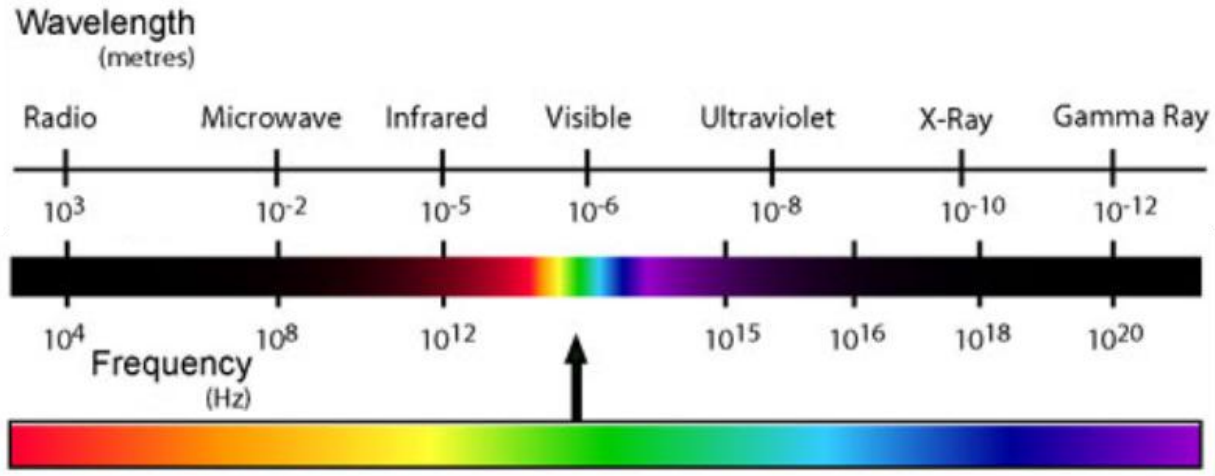

Figure 1.1 Electromagnetic Spectrum

However, this has a major disadvantage for the higher frequency waves because of its higher meanfree path loss according to the Friis free space equation which is given as

$$L \propto f^2 \tag{1-1}$$

where L is the mean free path loss of the electromagnetic wave and f is the frequency of the electromagnetic wave. This also enhances blockages and shadowing in terrestrial communication for electromagnetic waves at higher frequencies. Thus, research in recent times are being focused towards the improvement of line-of-sight (LoS) wireless communication. The visible light band in the electromagnetic spectra spans in the

frequency range of 400 THz to 800 THz and thus has much higher bandwidth than the radio spectra spanning from 3 kHz to 300 GHz. This has triggered the idea of using visible light to be used short range wireless communication.

Alexander Graham Bell in the 1880s made the first use of light for communication when modulated sunlight by using oscillating mirrors (called photophone) to transmit speech over several hundred meters[11]. Modern day visible light communication (VLC) uses a light emitting diode (LED) and laser diodes as a source to transmit modulated signals and a photodetector (or an array of photodetectors) to receive the signal. The LEDs having advantages of longer product life, lower heat dissipation and higher quantum efficiency are replacing incandescent bulbs and fluorescent lamps in commercial places and households. Also, they have very high switching speeds making them the ideal candidate to be used as a transmitter of data. Since this rapid switching of the intensity of the LEDs is invisible to the human eye, the LEDs can perform dual functionalities of illumination and high speed data transfer. In 2003, Tanaka and coworkers first used white LEDs for this dual purpose and used on-off keying (OOK) modulation technique to attain up to 400 Mbps data rate[12]. Orthogonal Frequency Division Multiplexing which is disadvantageous in RF communication can be used as an advantage in VLC was for the first time by shown by Afghani and coworkers[13]. Vucic *et al.* achieved a 500 Mbps data rate thus making VLC a potential candidate for wireless communication by using direct current biased optical (DCO) OFDM technique[14]. Wavelength division multiplexing (WDM) using a red, green and blue (RGB) white LED by separately modulating red, green and blue modes and employing respective filters at the receiver gave a data rate of 800 Mbps[15]. Khalid et al. presented a link implementation using DCO-OFDM and achieved 1 Gbps with single phosphor coated LED[16]. Later they also demonstrated a 3.4 Gbps link using off-the-shelf RGB LED[17]. The same data rate was demonstrated by Azhar et al using a 4 x 4 multi-input-multi-output (MIMO) configuration[18]. Recently, Tsonev demonstrated a 3.5 Gbps data rate using a single color μLED in a single input and single output (SISO) setting[19]. These developments promoted optical wave communication as the next generation of wireless technology and is called Light Fidelity (Li-fi) (a term coined by Harald Hass in 2011 at TED Global[20])

1.1.1 Advantages of Optical Wireless Communication

- Li-Fi does not cause any interference with RF signals and so this technology is tailor-made for indoor communication in offices, healthcare, industries and aerospace.
- Information embedded in light cannot penetrate the wall surfaces and thus the data is confined to room walls making Li-Fi highly secure.
- The light from LEDs is confined to a smaller area and highly directional. As a result, the existence of closely placed non-interfering transmitters is possible leading to better traffic handling capabilities and higher data densities.
- Visible light does not cause hazards under illumination conditions. Unlike RF, visible light satisfies the health-related safety regulations and does not cause complications. Hence, it is more suitable in situations where high power signals need to be transmitted.
- Very less energy is consumed by the LEDs and their switching rates can be controlled, making them excellent sources for modulation. The cost of implementation of VLC devices is very less.
- Simple electronic components operating in baseband may be used to implement Li-Fi by utilizing existing optic fiber infrastructure. This is given rise to greater interests in short range indoor communication using light.

1.1.2 Modulation Techniques

- *Single Carrier Modulation:* The most basic technique used in optical wireless communication is single carrier modulation (SCM). This was originally developed for intensity modulation and direct detection (IM/DD) of infra-red based communication systems[21]. SCM techniques are generally suitable where low to moderate data rate applications are required. The commonly used SCM technique is on-off keying (OOK) which uses a simple two amplitude level scheme to define high and low logic bits. OOK modulation technique supports dimmable illumination i.e., communication is enabled even when illumination is not required. OOK dimming is specified in IEEE 802.15.7 and is achieved by defining the ON/OFF amplitude and applying symbol compensation[22]. Pulse amplitude modulation (PAM), pulse position modulation (PPM) and pulse width modulation

(PWM) are the other common SCM techniques used in optical wireless communication[10,23].

- *Multi-Carrier Modulation:* The SCM technique suffers a limitation of requiring complex equalizers at the receiver end due to the dispersive nature of the optical wireless channels. However, the multi-carrier modulation (MCM) techniques, for example, orthogonal frequency division multiplexing (OFDM)[10,13,23,24] are one of the potential candidates for transmission of data as they require only a single tap equalizer at the receiver's end. In OFDM, parallel data streams are sent simultaneously through a collection of subcarriers and thus a complex equalization technique at the receiver's end can be omitted. Although they enhance the bandwidth of transmission of data, they are not very energy efficient.
- *Color Shift Keying:* The color shift keying (CSK) is generally used in red, green and blue (RGB) LED based lighting systems. It is an intensity modulated technique in which the incoming bits of data are encoded into the color intensities emitted by the RGB LEDs. This method is outlined in IEEE 802.15.7[22]. The output color, however, stays constant and the relative intensities between the multiple wavelengths are altered thus enhancing the bandwidth and data rate. They are advantageous over conventional intensity modulated schemes as a constant flux of light is guaranteed as there would be no flicker effect over all frequencies. Also, the constant luminous flux implies an almost constant LED driving current thus reducing the possible inrush of current at signal modulation improving LED reliability. Another advantage of using RGB LEDs is that they can be used as separate channels for uplink and downlink.

1.2 Photodiodes

1.2.1 Mode of Operation Of Photodiode

Photovoltaic Mode: In this mode, the photodiode is operated in zero bias condition. The charge carriers generated due to light signal gets extracted due to the built-in potential of the photodiode.

Photoconductive Mode: In this mode, the photodiode is operated in the presence of reverse bias. Due to the presence of the external reverse bias, the built-in potential increases and thus leads to efficient extraction of the charge carriers. This mode although enhances

responsivity, and reduces response time but increases the dark current thereby increases the noise floor of the photodiode.

1.2.2 Figures Of Merit Of Photodiode

Responsivity

The external quantum efficiency (EQE), also called as the incident photon to current efficiency (IPCE) is defined as the ratio of the number of electrons extracted from the electrodes to the number of photons incident. The more practical unit of EQE is responsivity which is the ratio of the output current to the incident power of light. The unit of responsivity is Amperes/Watt (A/W). The responsivity (R) and EQE is given as follows[25]:

$$\boldsymbol{R = \frac{J_{ph}}{L_{in}}} \qquad \textit{(1-2)}$$

$$\boldsymbol{EQE = \frac{Rhc}{\lambda e}} \qquad \textit{(1-3)}$$

where J_{ph} is the photocurrent density, L_{in} is the incident light irradiance, e is the elementary charge and hc/λ is the energy of incident photon. If a constant light source is assumed that is the number of photons per unit time is fixed the EQE is entirely determined by the photocurrent.

Dark And Noise Current

The dark current is defined as the current flowing through the device in the absence of light in the photoconductive mode. The dark current is dependent mainly on the electronic properties of the device such as the mobility of electrons and holes, trap density, doping and the work functions of the electrodes[26]. For an ideal photodetector, the dark current should be as low as possible (~1 - 1000 nA). It has been seen by the use of thick active layers[27,28], use of electron-hole blocking layers[29,30] the dark currents can be reduced substantially. The noise level can be defined as the current generated in the absence of light signal.

The noise current, i_{noise} which is the root mean square of the fluctuations in dark current of the photodiode can be written in a general form at a detection bandwidth B[25]:

$$\boldsymbol{i_{noise} = \left[i_{shot}^2 + i_{thermal}^2 + i_{1/f}^2 + i_{g-r}^2\right]^{\frac{1}{2}}}$$

$$= \left[2ei_dB + \frac{4K_BTB}{R_{sh}} + i(f.B)^2_{1/f} + i(f.B)^2_{g-r}\right]^{\frac{1}{2}} \qquad (1\text{-}4)$$

where K_B is the Boltzmann constant, T the absolute temperature and R_{sh} the shunt resistance of the photodiode.

The spectra of the first two terms shot noise and thermal noise in the expression are "white" that is they are independent of frequency. The third and fourth terms are the frequency dependent noise components referred conventionally as the $1/f$ noise[31] and generation recombination noise[32] respectively.

Noise Equivalent Power and Specific Detectivity

Noise equivalent power (NEP) is defined as the minimum power of light that can be detected by a photodiode at a signal to noise ratio of one (S/N ~ 1) when the electrical bandwidth is equal to one. In other words, it is the power corresponding to the noise current. The NEP in units of $W/\sqrt{Hz}$ can be written in terms of responsivity R and bandwidth B as[25]

$$NEP = \frac{i_{noise}}{R\sqrt{B}} \qquad (1\text{-}5)$$

Detectivity, D is the reciprocal of the noise equivalent power (NEP). It can be normalized to the square root of active area of the device, A thus obtaining the specific detectivity, D^* of the photodiode in units of $cm\ Hz^{1/2}W^{-1}$. Thus

$$D^* = \frac{\sqrt{A}}{NEP} = \frac{R\sqrt{AB}}{i_{noise}} \qquad (1\text{-}6)$$

Using equations (1-4) and (1-7), D^* can be expressed in terms of EQE[25]

$$D^* = e\lambda\sqrt{AB}.\frac{EQE}{hci_{noise}} \qquad (1\text{-}7)$$

There are mainly two methods to increase the specific detectivity of the photodiodes either by increasing the EQE (responsivity) or by suppressing the noise current. However, by increasing the active area of the device enhances the EQE but also results in the increase of the dark current thereby increasing noise compromising D^*.

Dynamic Range

The dynamic range of a photodiode quantifies the ability of the photodetector to capture the variation in light intensities. In order for the photodiodes to be used in real life, a linear dynamic range (LDR) is desired i.e., the photocurrent versus intensity is linear function [33,34]. Mathematically it is defined as[25]

$$\boldsymbol{LDR = 20log(I_{max}/I_{min})} \qquad \textit{(1-8)}$$

Where I_{max} and I_{min} are the maximum and minimum photocurrents in the linear region of intensity versus photocurrent curve.

At low light intensities, the bimolecular recombination (i.e., when the recombination rate is quadratically proportional to the carrier density) is negligible to the extraction rate, the photocurrent is linear with respect to the light intensity. As the light intensity increases, the photocurrent will deviate from linearity at a certain light intensity and photocurrent J_{max} depending on the charge mobility of the active materials[34] and recombination rate coefficient[35]. The reason behind this is mainly due to the formation of space charges when the concentration of charge carrier increases resulting in the lowering of bimolecular lifetime in comparison to the transit time of the charge carriers[34,35].

In general, to improve the LDR the noise levels can be lowered for I_{min} . Increase in the space charge formation threshold results in the increase of I_{max}. In OPD this can be achieved as: increase in the slower carrier mobility[34], decrease in the junction thickness[34], minimization of the series resistance[34], and use of donor acceptor systems with suppressed bimolecular recombination[35].

Speed Of Response

The time taken to extract the generated electrons and holes corresponds to the speed of response. The temporal bandwidth is defined as the frequency of incident modulation of light at which the response of the photodiode is -3 dB lower than the continuous wave response. The -3dB bandwidth is limited by the characteristic RC time constant and the carrier transit time or both[36]. It is given by[25]

$$\frac{\mathbf{1}}{\boldsymbol{f^2_{-3dB}}} = \frac{\mathbf{1}}{\boldsymbol{f^2_t}} + \frac{\mathbf{1}}{\boldsymbol{f^2_{RC}}} \qquad \textit{(1-9)}$$

where f_t and f_{RC} are the carrier transit time limited bandwidth and RC limited bandwidth respectively and are defined as

$$f_t = \frac{3.5}{2\pi t_{1r}} \quad (1\text{-}10)$$

$$f_{RC} = \frac{1}{2\pi RC} \quad (1\text{-}11)$$

Where t_{1r} is the carrier transit time, R the total series resistance including photodiode series resistance, contact resistances, sheet resistance and load resistance in the measurement circuit. Decreasing the active layer thickness can potentially increase the frequency bandwidth as transit time is given as[25]

$$t_{1r} = \frac{d^2}{\mu V} \quad (1\text{-}12)$$

where d is the active layer thickness, μ is the charge carrier mobility and V is voltage which is essentially the sum of the applied voltage and the built-in voltage.

1.3 Polymer Semiconductor

Organic semiconductors are conjugated systems where carbon atoms are linked by alternate single and double bonds. In a conjugated system, 2s, $2p_x$ and $2p_y$ hybridize to form three sp^2 orbitals which form sigma bonds with other atoms. The unhybridized $2p_z$ orbital is in the plane perpendicular to the plane of the hybridized sp^2 orbital and carries one unpaired electron. The neighboring $2p_z$ orbitals overlap to form a delocalized π electron cloud. This electron delocalization in the plane perpendicular to the plane of sigma bonds generally acts as free electrons in the conjugated backbone.

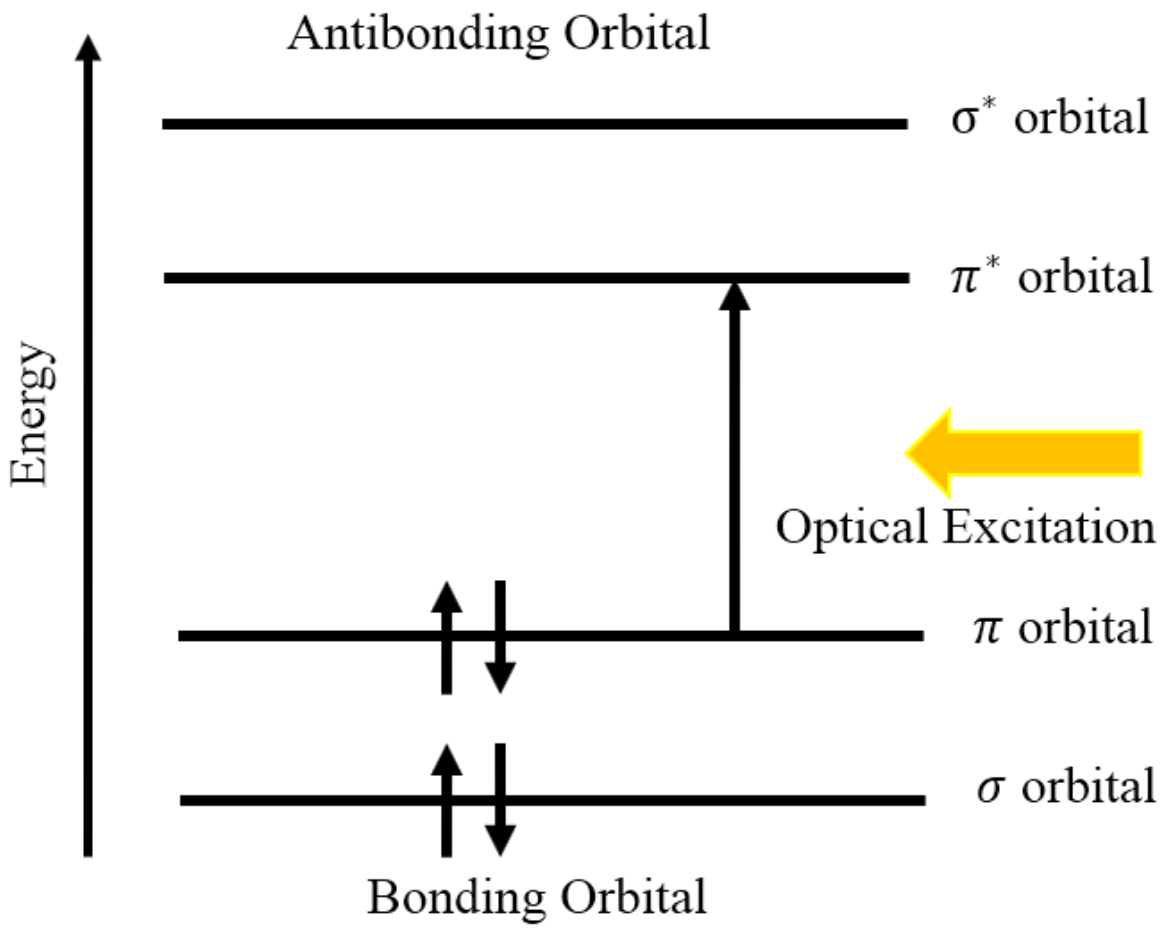

Figure 1.2: Energy Levels of a π conjugated system

Peirels instability [37] is the phenomenon in which any symmetric 1-D electronic structure is unstable due to the doubling of the unit cell. Such doubling of the unit cell causes an opening of energy gap at the Fermi level. Thus, in a symmetric 1-D electron distribution this delocalized electron clouds form alternate single and double bonds. This rearrangement of electron cloud along the polymer backbone gives rise to the formation of delocalized energy bands called the bonding (π) and anti-bonding (π^*) orbital. Generally the bonding orbital is lower in energy and is called as the Highest Occupied Molecular Orbital (HOMO) and the anti-bonding orbital is termed as the Lowest Unoccupied Molecular Orbital (LUMO) [38,39]. The energy gap between the HOMO and LUMO has a value of 1-3 eV and so this type systems by definition are semiconductors.

A polymer is ideally a chain of alternately single and double bonded carbon atoms of different length. Cornil et al. studied the effect of chain length on the HOMO-LUMO level

splitting [40]. The average energy gap reduces further when the polymers are stacked as films by Van der Waals interaction.

Table 1.1: Properties of some important organic semiconductors

Semiconductors	Band Gap (eV)	HOMO (eV)	LUMO (eV)	Mobility (hole) (cm^2/Vs)
P3HT	1.9	-3.0	-4.9	~10^{-4} [41]
PBTTT-C14	2.0	-3.46	-5.46	~0.2-0.6 (μFET)[42]
PDBTTT-C-T	1.68	-3.6	-5.28	~10^{-3} [43]
PFO	3.2	-5.8	-2.6	~10^{-3} [44]
PCBM-C60	2.1	-3.9	-6.0	~10^{-3} [45]

The decrease in the gap by increasing length of the polymer chain by using a very simple model of a semi-classical particle trapped in a 1-D box. In this case, the delocalized π electrons act as particles in the 1-D box. For a box of length L, the energy levels and difference in the energy levels are given by

$$\boldsymbol{E_n = \frac{\hbar^2\pi^2}{2m_eL^2}n^2} \text{ and } \boldsymbol{\Delta E = \frac{\hbar^2\pi^2}{2m_eL^2}(2n+1)} \qquad \textit{(1-13)}$$

A polymer of length L as a chain of $2N$ recurring units each of length a is considered. If each monomer contributes $m\pi$ electrons, then the total number of state occupied are $Nm/2$. Thus

$$\boldsymbol{\Delta E = \frac{\hbar^2\pi^2}{2m_eL^2(Na)^2}\left(2\left(\frac{Nm}{2}\right)+1\right) = \frac{\hbar^2\pi^2}{2m_ea^2}\left(\frac{m}{N}+\frac{1}{N^2}\right) \propto \frac{1}{N}} \qquad \textit{(1-14)}$$

Thus, the gap between the consecutive levels is inversely proportional to the length of the polymer chain.

Comparison of Polymer and Inorganic Semiconductors

- Organic semiconductors have charge carrier mobility ($\mu \sim 10^{-2}$ to 10^{-5} $cm^2/V.s$)[46] which is 10^4 to 10^6 lesser than the inorganic semiconductors ($\mu \sim 10^2$ to 10^4 $cm^2/V.s$)[47].
- Diffusion lengths of primary excitons (electrostatically bound state of an electron and hole) in disordered organic materials (L_D~5-10 nm)[48] is very less compared to the diffusion length of charge transport in inorganic semiconductors (L_D(Si) ~ 700 nm, L_D(GaAs) ~ 10 μm).
- Organic semiconducting materials have higher absorption coefficient ($\alpha \geq 10^5$ cm^{-1})[49] compared to inorganic semiconductors ($\alpha \geq 10^4 cm^{-1}$)[50].
- The band gap of organic semiconductors can be easily tuned at a low cost. Band gap tuning is also possible for InAlGaN family, but it is highly costly.
- Organic materials are useful alternatives to their inorganic counterparts due to the ease of fabrication and much lower cost.

1.4 Organic Photodiodes

Organic photodiodes (OPD) has the potential to meet the present and future needs of photodiodes because of their ease of fabrication, flexibility, responsivity spectra tunability and low cost.

The first OPD was demonstrated by Kudo and Moriizumi in 1981[51]. Merocyanine/Rhodamine B bilayer was used as the active component in the photodiode. Merocyanine was used as the donor type material (p-type material) and Rhodamine B as the acceptor type material (n-type material).

In OPD, the incident light from the source is absorbed as the photons travel through the active layer of the organic semiconductor. The absorption only happens when the band gap of the semiconductor is equal or lower than the energy of the incident photons. The organic semiconductors are generally media with low dielectric constant (ϵ~3-4). This leads to the formation of a neutral bound-state entity called an exciton (a bound state of an electron and a hole held together by Coulombic attraction) rather than free charges. The separation of the exciton into a free electron and a hole is due to the weak screening of the Coulombic attraction of the electron hole pair. Due to this the quantum yield of free generation of

carriers is low for a homojunction (an active layer comprised of neat pristine material) which results in the external quantum efficiency at short circuit voltage being very poor (~1%). Thus, strategies to overcome the exciton binding energies (~0.3 - 0.5 eV) which is much higher for room temperature [52] thermal energy (K_BT) are essential to obtain high EQE. The most widely used approach to achieve free charge carrier generation in OPDs is to combine an electron donor and an acceptor such that the donor acceptor energy offset is greater the exciton binding energy for electron and hole transfer to occur. This can be achieved in two ways:

- Forming a donor-acceptor planar heterojunction (a 'bilayer')[51]
- Mixing a donor-acceptor in a blend to form a distributed heterojunction in the bulk of the active layer (bulk heterojunction (BHJ) layer)[53,54].

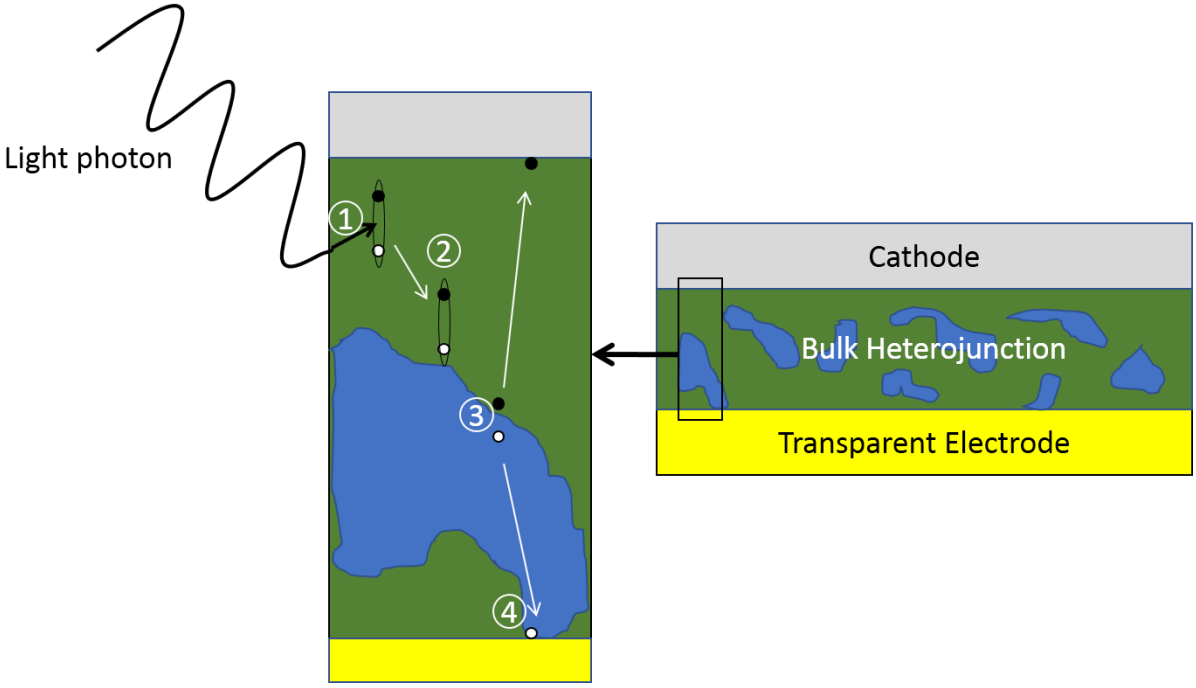

Figure 1.3: Working Of an organic BHJ photodiode

The second method is the most successful method of charge carrier separation and has brought a revolution in the field of organic solar cells (OSC) and organic photodiodes (OPD). Their working principle can be summarized as follows

- Absorption of photon by donor species and creation of exciton
- Diffusion of exciton to donor-acceptor interface
- Exciton dissociation at the interface and formation of charge transfer state, which subsequently dissociates to form free charge carriers.

- Diffusion of separated charges to the respective electrodes

OPDs have matched and outperformed silicon in a range of metrics including the linear dynamic range (LDR)[55,56], specific detectivity[57], the speed of response[58], dark current[59] and spectrally flat internal quantum efficiencies (IQE)[60]. Organic materials allow photodiodes to be fabricated onto a mechanically flexible substrates[61-63], large surfaces[64] or used as ultra-thin devices[65].

The speed of response or the temporal bandwidth OPD holds a major importance for them to be used in VLC. For OPDs the temporal bandwidths have been reported for different wavelengths:430 MHz for wavelength between 500nm to 750nm[66], 100 kHz to 1 MHz for visible spectrum[27,67] and 10 to 100 MHz for blue sensitive photodiodes[68].

1.5 Overview Of the Thesis

The thesis focusses mainly on the fabrication of organic photodiodes to be used as potential detectors for VLC. Chapter 2 deals with a binary blend bulk heterojunction (BHJ) based organic photodiode consisting of poly(9,9-dioctylfluorenyl-2,7-diyl) (PFO) as the donor and [6-6]phenyl-C61-butyric acid methylester (PCBM) as the acceptor that was fabricated to so that the detector has high responsivity and temporal response in the blue region. The fabrication protocols and characterization of the OPD are given in the chapter.

To enhance the temporal response and responsivity in the near infra-red (NIR) a NIR dye was added to this binary blend which is discussed in Chapter 3. Apart from PFO, a squaraine derivative with a very narrow absorption range in the NIR region was used to fabricate the OPD. The addition of this squaraine derivative enhanced the responsivity and bandwidth of the photodiode. The fabrication protocols and characterization of the ternary blend OPD are focused in the chapter.

Chapter 4 deals with the influence of various coatings on the wall (both phosphorescent and fluorescent) in the non-line of sight visible light communication. The enclosure boundary normally is treated as a classical light diffuser which merely scatters and attenuates the signal[69,70]. The use of various photo-luminescent coatings on walls acts as active noise sources which distort the signal and alter the communication characteristics[71-73]. The possibility of tuning the signal to noise levels by these emitters as a function of the spatial coordinates can be utilized to design smart environments where signal access can be controlled and restricted. Conversely, the signal analysis can also be utilized to provide

dynamic information about the environment. The chapter also deals with the feasibility of VLC in dark conditions after the primary LEDs are switched off, which depends upon the emission persisting for a sufficiently long duration, and can also lead to novel applications.

1.6 References

1 Faraday, M. *Experimental researches in electricity*. Vol. 1 (Read Books Ltd, 2016).

2 Ross, I. M. The invention of the transistor. *Proceedings of the IEEE* **86**, 7-28 (1998).

3 Ghioni, M., Zappa, F., Kesan, V. P. & Warnock, J. A VLSI-compatible high-speed silicon photodetector for optical data link applications. *IEEE Transactions on Electron Devices* **43**, 1054-1060 (1996).

4 Tang, C. W. & VanSlyke, S. A. Organic electroluminescent diodes. *Applied physics letters* **51**, 913-915 (1987).

5 Burroughes, J. *et al.* Light-emitting diodes based on conjugated polymers. *nature* **347**, 539-541 (1990).

6 Padinger, F., Rittberger, R. S. & Sariciftci, N. S. Effects of postproduction treatment on plastic solar cells. *Advanced Functional Materials* **13**, 85-88 (2003).

7 Reyes-Reyes, M., Kim, K. & Carroll, D. L. High-efficiency photovoltaic devices based on annealed poly (3-hexylthiophene) and 1-(3-methoxycarbonyl)-propyl-1-phenyl-(6, 6) C 61 blends. *Applied Physics Letters* **87**, 083506 (2005).

8 Drury, C., Mutsaers, C., Hart, C., Matters, M. & De Leeuw, D. Low-cost all-polymer integrated circuits. *Applied Physics Letters* **73**, 108-110 (1998).

9 Emerson, D. T. The work of Jagadis Chandra Bose: 100 years of millimeter-wave research. *IEEE transactions on microwave theory and techniques* **45**, 2267-2273 (1997).

10 Haas, H., Yin, L., Wang, Y. & Chen, C. What is LiFi? *Journal of Lightwave Technology* **34**, 1533-1544 (2016).

11 Bell, A. G. Selenium and the Photophone. *Nature* **22**, 500-503 (1880).

12 Tanaka, Y., Komine, T., Haruyama, S. & Nakagawa, M. Indoor visible light data transmission system utilizing white LED lights. *IEICE transactions on communications* **86**, 2440-2454 (2003).

13 Afgani, M. Z., Haas, H., Elgala, H. & Knipp, D. in *Testbeds and Research Infrastructures for the Development of Networks and Communities, 2006. TRIDENTCOM 2006. 2nd International Conference on.* 6 pp.-134 (IEEE).

14 Vucic, J., Kottke, C., Nerreter, S., Langer, K.-D. & Walewski, J. W. 513 Mbit/s visible light communications link based on DMT-modulation of a white LED. *Journal of lightwave technology* **28**, 3512-3518 (2010).

15 Vučić, J., Kottke, C., Habel, K. & Langer, K.-D. in *Optical Fiber Communication Conference and Exposition (OFC/NFOEC), 2011 and the National Fiber Optic Engineers Conference.* 1-3 (IEEE).

16 Khalid, A., Cossu, G., Corsini, R., Choudhury, P. & Ciaramella, E. 1-Gb/s transmission over a phosphorescent white LED by using rate-adaptive discrete multitone modulation. *IEEE Photonics Journal* **4**, 1465-1473 (2012).

17 Cossu, G., Khalid, A., Choudhury, P., Corsini, R. & Ciaramella, E. 3.4 Gbit/s visible optical wireless transmission based on RGB LED. *Optics express* **20**, B501-B506 (2012).

18 Azhar, A. H., Tran, T. & O'Brien, D. A gigabit/s indoor wireless transmission using MIMO-OFDM visible-light communications. *IEEE Photonics Technology Letters* **25**, 171-174 (2013).

19 Tsonev, D. *et al.* A 3-Gb/s single-LED OFDM-based wireless VLC link using a gallium nitride μLED. *IEEE Photon. Technol. Lett.* **26**, 637-640 (2014).

20 Haas, H. *Harald Haas: Wireless data from every light bulb*. (TED, 2011).

21 Kahn, J. M. & Barry, J. R. Wireless infrared communications. *Proceedings of the IEEE* **85**, 265-298 (1997).

22 IEEE Standard for Local and Metropolitan Area Networks--Part 15.7: Short-Range Wireless Optical Communication Using Visible Light. *IEEE Std 802.15.7-2011*, 1-309, doi:10.1109/IEEESTD.2011.6016195 (2011).

23 Islim, M. S. & Haas, H. Modulation Techniques for Li□ Fi. *ZTECOMMUNICATIONS*, 29 (2016).

24 Komine, T., Haruyama, S. & Nakagawa, M. in *Wireless Pervasive Computing, 2006 1st International Symposium on.* 6 pp.-6 (IEEE).

25 Jansen-van Vuuren, R. D., Armin, A., Pandey, A. K., Burn, P. L. & Meredith, P. Organic photodiodes: the future of full color detection and image sensing. *Advanced Materials* **28**, 4766-4802 (2016).

26 Wetzelaer, G., Kuik, M., Lenes, M. & Blom, P. Origin of the dark-current ideality factor in polymer: fullerene bulk heterojunction solar cells. *Applied Physics Letters* **99**, 153506 (2011).

27 Armin, A. *et al.* Thick junction broadband organic photodiodes. *Laser & Photonics Reviews* **8**, 924-932 (2014).

28 Ramuz, M., Bürgi, L., Winnewisser, C. & Seitz, P. High sensitivity organic photodiodes with low dark currents and increased lifetimes. *Organic Electronics* **9**, 369-376 (2008).

29 Gong, X. *et al.* Semiconducting polymer photodetectors with electron and hole blocking layers: High detectivity in the near-infrared. *Sensors* **10**, 6488-6496 (2010).

30 Lyons, D. M. *et al.* Narrow band green organic photodiodes for imaging. *Organic Electronics* **15**, 2903-2911 (2014).

31 Dereniak, E. L. & Boreman, G. D. *Infrared detectors and systems*. (Wiley, 1996).

32 Balandin, A. A. *Noise and fluctuations control in electronic devices*. (Amer. sci. publ. Stevenson Ranch (Ca), 2002).

33 Konstantatos, G., Clifford, J., Levina, L. & Sargent, E. H. Sensitive solution-processed visible-wavelength photodetectors. *Nature photonics* **1**, 531-534 (2007).

34 Stolterfoht, M. *et al.* Photocarrier drift distance in organic solar cells and photodetectors. *Scientific reports* **5**, 9949 (2015).

35 Jin, H. *et al.* Bulk heterojunction thickness uniformity–a limiting factor in large area organic solar cells? *physica status solidi (a)* **212**, 2246-2254 (2015).

36 El-Desouki, M. *et al.* CMOS image sensors for high speed applications. *Sensors* **9**, 430-444 (2009).

37 Peierls, R. E. *Quantum theory of solids*. (Oxford University Press, 1955).

38 Chamberlain, G. Organic solar cells: A review. *Solar cells* **8**, 47-83 (1983).

39 Hertel, D. & Bässler, H. Photoconduction in amorphous organic solids. *ChemPhysChem* **9**, 666-688 (2008).

40 Cornil, J., Beljonne, D., Calbert, J. P. & Brédas, J. L. Interchain interactions in organic π-conjugated materials: impact on electronic structure, optical response, and charge transport. *Advanced materials* **13**, 1053-1067 (2001).

41 Baumann, A., Lorrmann, J., Deibel, C. & Dyakonov, V. Bipolar charge transport in poly (3-hexyl thiophene)/methanofullerene blends: A ratio dependent study. *Applied Physics Letters* **93**, 252104 (2008).

42 McCulloch, I. *et al.* Liquid-crystalline semiconducting polymers with high charge-carrier mobility. *Nature materials* **5**, 328-333 (2006).

43 Kim, H. *et al.* Regioregular low bandgap polymer with controlled thieno [3, 4-b] thiophene orientation for high-efficiency polymer solar cells. *Chemistry of Materials* **27**, 3102-3107 (2015).

44 Babel, A. & Jenekhe, S. A. Charge Carrier Mobility in Blends of Poly(9,9-dioctylfluorene) and Poly(3-hexylthiophene). *Macromolecules* **36**, 7759-7764, doi:10.1021/ma034717t (2003).

45 von Hauff, E., Dyakonov, V. & Parisi, J. Study of field effect mobility in PCBM films and P3HT: PCBM blends. *Solar energy materials and solar cells* **87**, 149-156 (2005).

46 Tiwari, S. & Greenham, N. Charge mobility measurement techniques in organic semiconductors. *Optical and quantum electronics* **41**, 69-89 (2009).

47 Chin, V., Tansley, T. & Osotchan, T. Electron mobilities in gallium, indium, and aluminum nitrides. *Journal of Applied Physics* **75**, 7365-7372 (1994).

48 Shaw, P. E., Ruseckas, A. & Samuel, I. D. Exciton diffusion measurements in poly (3-hexylthiophene). *Advanced Materials* **20**, 3516-3520 (2008).

49 Peumans, P., Yakimov, A. & Forrest, S. R. Small molecular weight organic thin-film photodetectors and solar cells. *Journal of Applied Physics* **93**, 3693-3723 (2003).

50 Murata, K. *et al.* Photogenerated polarons in poly (paraphenylene vinylene). *Chemical physics* **227**, 191-201 (1998).

51 Kudo, K. & Moriizumi, T. Spectrum-controllable color sensors using organic dyes. *Applied Physics Letters* **39**, 609-611 (1981).

52 Knupfer, M. Exciton binding energies in organic semiconductors. *Applied Physics A: Materials Science & Processing* **77**, 623-626 (2003).

53 Park, S. H. *et al.* Bulk heterojunction solar cells with internal quantum efficiency approaching 100%. *Nature photonics* **3**, 297-302 (2009).

54 Yu, G., Gao, J., Hummelen, J. C., Wudl, F. & Heeger, A. J. Polymer photovoltiac cells: Enhanced efficiencies via a network of internal donor-acceptor heterojunctions. *Science* **270**, 1789 (1995).

55 Gong, X. *et al.* High-detectivity polymer photodetectors with spectral response from 300 nm to 1450 nm. *Science* **325**, 1665-1667 (2009).

56 Guo, F., Xiao, Z. & Huang, J. Fullerene Photodetectors with a Linear Dynamic Range of 90 dB Enabled by a Cross-Linkable Buffer Layer. *Advanced Optical Materials* **1**, 289-294 (2013).

57 Su, Z. *et al.* High-Performance Organic Small-Molecule Panchromatic Photodetectors. *ACS applied materials & interfaces* **7**, 2529-2534 (2015).

58 Yang, D. & Ma, D. 1, 1-Bis [(di-4-tolylamino) phenyl] cyclohexane for fast response organic photodetectors with high external efficiency and low leakage current. *Journal of Materials Chemistry C* **1**, 2054-2060 (2013).

59 Leem, D.-S. *et al.* Low dark current inverted organic photodetectors employing MoOx: Al cathode interlayer. *Organic Electronics* **24**, 176-181 (2015).

60 Armin, A. *et al.* Spectral dependence of the internal quantum efficiency of organic solar cells: Effect of charge generation pathways. *Journal of the American Chemical Society* **136**, 11465-11472 (2014).

61 Someya, T. *et al.* Integration of organic FETs with organic photodiodes for a large area, flexible, and lightweight sheet image scanners. *IEEE transactions on electron devices* **52**, 2502-2511 (2005).

62 Kraker, E. *et al.* Organic photodiodes on flexible substrates. *Thin Solid Films* **518**, 1214-1217 (2009).

63 Lamprecht, B., Thünauer, R., Ostermann, M., Jakopic, G. & Leising, G. Organic photodiodes on newspaper. *physica status solidi (a)* **202**, R50-R52 (2005).

64 Arca, F. *et al.* Interface trap states in organic photodiodes. *Scientific reports* **3**, 1324 (2013).

65 Liu, Z. *et al.* Transparent conductive electrodes from graphene/PEDOT: PSS hybrid inks for ultrathin organic photodetectors. *Advanced Materials* **27**, 669-675 (2015).

66 Peumans, P., Bulović, V. & Forrest, S. Efficient, high-bandwidth organic multilayer photodetectors. *Applied Physics Letters* **76**, 3855-3857 (2000).

67 Baierl, D., Fabel, B., Lugli, P. & Scarpa, G. Efficient indium-tin-oxide (ITO) free top-absorbing organic photodetector with highly transparent polymer top electrode. *Organic Electronics* **12**, 1669-1673 (2011).

68 Hamasaki, T. *et al.* Fabrication and characteristics of polyfluorene based organic photodetectors using fullerene derivatives. *Thin Solid Films* **518**, 548-550 (2009).

69 Chung, Y. H. & Oh, S.-b. in *Intelligent Signal Processing and Communications Systems (ISPACS), 2013 International Symposium on.* 749-752 (IEEE).

70 Zhao, Y. & Vongkulbhisal, J. Design of visible light communication receiver for on-off keying modulation by adaptive minimum-voltage cancelation. *Engineering Journal* **17**, 125-130 (2013).

71 Chow, C., Yeh, C., Liu, Y. & Huang, P. Mitigation of optical background noise in light-emitting diode (LED) optical wireless communication systems. *IEEE photonics Journal* **5**, 7900307-7900307 (2013).

72 Sindhubala, K. & Vijayalakshmi, B. Review On Impact Of Ambient Light Noise Sources And Applications In Optical Wireless Communication Using LED. *International Journal of Applied Engineering Research* **10**, 31115-31130 (2015).

73 Liu, Y., Yeh, C., Wang, Y. & Chow, C. in *OptoElectronics and Communications Conference and Photonics in Switching.* TuPR_10 (Optical Society of America).

CHAPTER 1

CHAPTER 1

CHAPTER 2

CHARACTERISTICS OF BINARY BLEND PFO:PCBM BHJ PHOTODIODES

The main goal of this chapter is to fabricate a photodiode having high responsivity and temporal response in the blue region. For this, a binary blend bulk heterojunction (BHJ) based organic photodiode consisting of poly(9,9-dioctylfluorenyl-2,7-diyl) (PFO) as the donor and [6-6]phenyl-C61-butyric acid methylester (PCBM) as the acceptor was fabricated. The fabrication protocols and characterization of the OPD are given in this chapter.

2.1 Materials

2.1.1 Donor Molecule (PFO)

Donor molecules are hole transporting organic materials. Semiconducting polymers consist of conjugated carbon chains in which adjacent chains are held by Van der Waal's interaction. Charge transport in semiconducting polymer systems is primarily along the backbone of the chain. Inter-chain hole-mobility is generally lower than hole mobility along a chain because of better overlap of the electron wavefunction within a chain than in between chains. PFO, a hole transporting polymer has been widely studied due to its photoluminescence properties[1,2] which enabled fabrication of blue organic light emitting diodes (OLEDs)[3-5]. It has a very narrow absorption range from 330 nm to 460 nm making it an ideal contender to be used as a donor material to make blue sensitive organic photodiodes[6]. The HOMO of the polymer is ~ -5.8 eV, while LUMO lies ~-2.6 eV. The band-gap of the polymer is ~ 3.2eV with an absorption maximum at 390 nm. PFO was used in this study for fabricating photodiodes. It was procured from Luminescent Technologies, Taiwan. Figure 2.3b shows its structure.

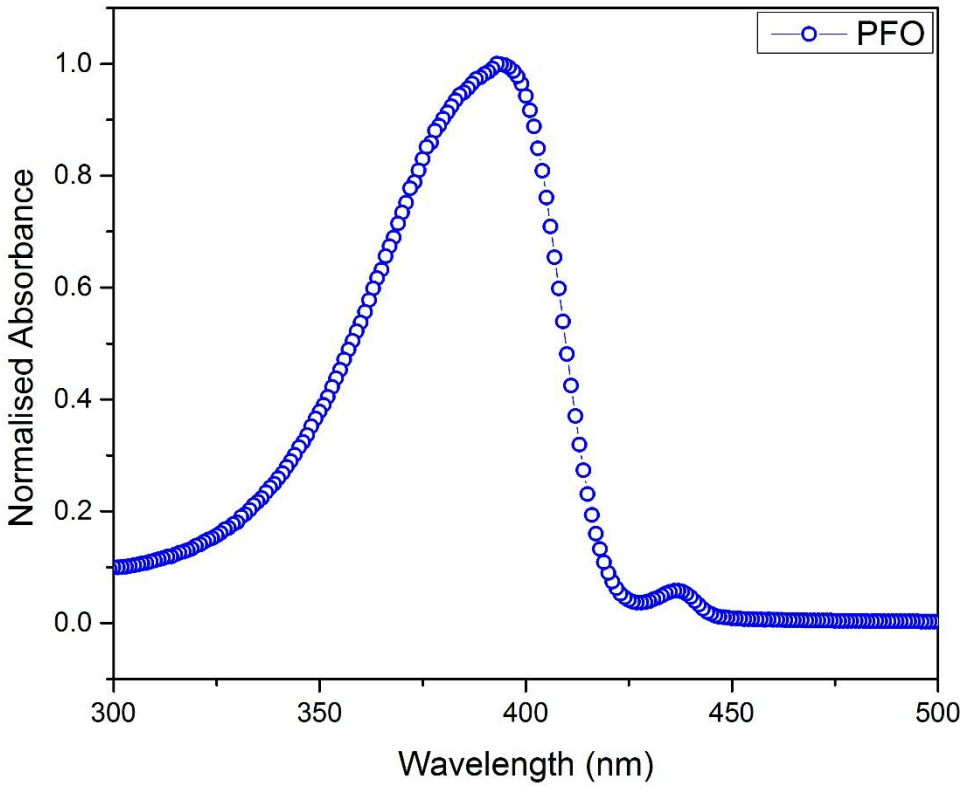

Figure 2.1: Absorption spectrum of PFO

2.1.2 Acceptor Molecule ($PC_{60}BM$)

Acceptor molecules are electron transporting organic materials and are usually small molecule systems. Fullerene-based acceptors are most successful and commonly used acceptors[7]. Since they are easily processible and have optimum band levels, they make excellent candidates to be used with various donors to fabricate solar cells and photodiodes. [6,6]-phenyl-C_{61}-butyric acid methyl ester ($PC_{60}BM$) (Figure 2.3a) is a small molecule derivative of fullerene[8]. This molecule which functions as an acceptor has its HOMO and LUMO close to -6.0 eV and -3.9 eV respectively. This makes the molecule to have a bandgap of 2.1 eV. The molecule absorbs in the wavelength range of 200 nm to 400 nm with absorption maximum around 270nm. Glass transition temperature of this molecule is found[9] to be 131.2^{o}C. $PC_{60}BM$ was purchased from Luminescent Technologies, Taiwan.

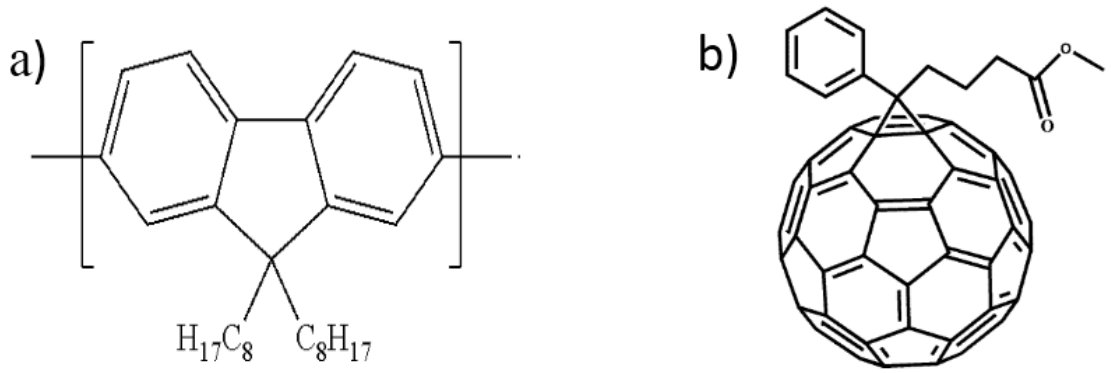

Figure 2.2: a) Structure of PFO b) Structure of $PC_{60}BM$

2.1.3 Buffer Layers

Buffer layers are introduced between the active layer and electrodes as functional layers to enhance charge carrier extraction[10]. The layers are generally selected depending on their energy levels and carrier mobilities. They can be both organic and inorganic materials. They are classified into electron buffer layers and hole buffer layers depending upon the carrier charge they allow.

2.1.3.1 Hole Buffer Layer

The hole-conducting buffer layers enhance the hole collection efficiency at the anode. These layers block transport of electrons through them. The necessary criterion for a material to act as a hole-buffer layer is that its HOMO level should be intermediate between donor HOMO and the work function of the hole-collecting electrode.

The hole buffer layer in our study was Molybdenum Oxide which is inorganic in nature[11]. Molybdenum Oxide has HOMO of around -5.3 eV and LUMO of around -2.4 eV. This is usually thermally evaporated. It has been seen[12] that when this is used as the hole-buffer layer it improves the long-term stability of the device. It is a common hole-buffer layer in organic devices with an inverted structure.

2.1.3.2 Electron Buffer Layer

Electron buffer layers are hole blocking layers and they are very efficient electron transport layers thereby increasing the efficiency of collection of electrons at the cathode. They also act as hole blocking layers. The LUMO of the buffer layer should be close to the work-function of electron collecting electrode. Zinc Oxide is the electron buffer layer[13] used in our study. It has HOMO of -7.5 eV and LUMO of -4.1 eV.

2.1.4 Electrodes

For optimum charge collection, electrodes of optimum work function are essential. In inverted structure devices, transparent Indium Tin Oxide (ITO) coated on glass acts as an electron collecting electrode and silver as the hole collecting electrode. The work functions of ITO and silver are -4.7eV and -4.73eV respectively.

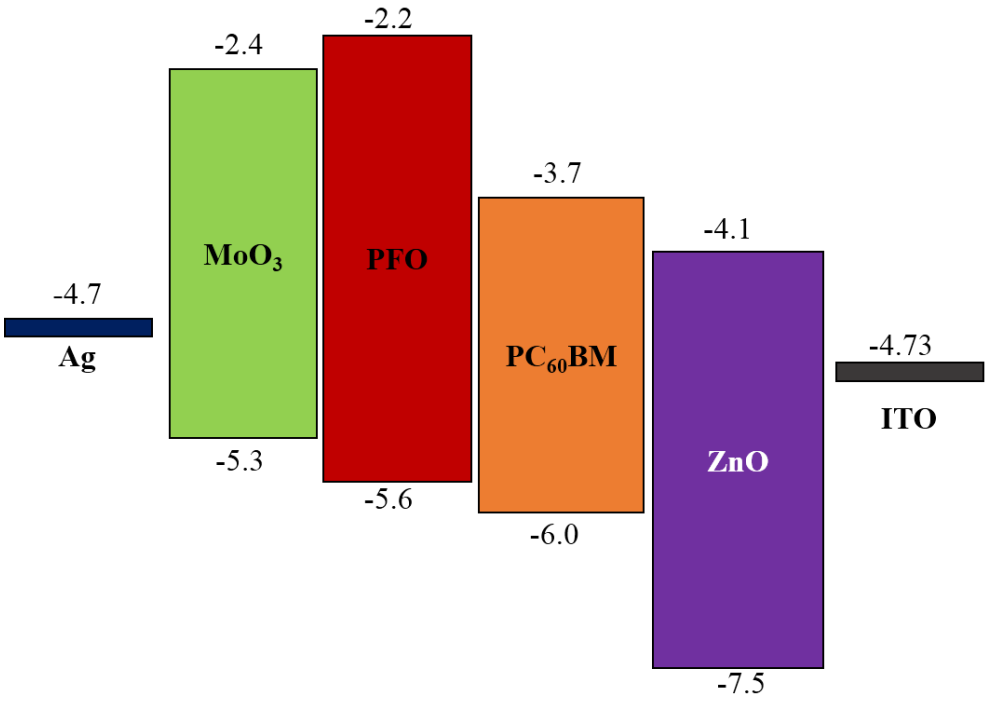

Figure 2.3: Energy level diagram of the layers used in the device

2.2 Organic Photodiode Fabrication

PFO:$PC_{60}BM$ photodiodes used in this report were fabricated in the inverted structure configuration. ZnO nanoparticles (NP) acted as the electron buffer layer and MoO_3 as the hole buffer layer. ITO and silver act as the electron collecting and hole collecting electrodes respectively. The steps involved in the fabrication of photodiodes are briefly discussed.

2.2.1 Etching of ITO

ITO coated glass slides are first masked with scotch tape in the region where it has to be etched. On the unmasked or the exposed area, concentrated hydrochloric acid with Zn dust is applied with cotton swabs. This was done till the glass slide does not reflect any color. More the dilution of the acid the slower is the etching process and thus it gives better control. Care should be taken that the acid does not seep to the masked part of the ITO.

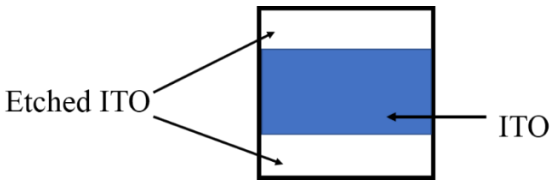

Figure 2.4: Etching of ITO

2.2.2 Cleaning Of ITO coated slides

The slides are initially cleaned with Extran solution to remove the dust. It was then further cleaned in IPA-acetone solution and blow dried with an air gun.

RCA treatment

De-ionized (DI) water of measured volume is pre-heated in a petri-dish to around 95^{o}C. Hydrogen peroxide and ammonia solution were added such that the volume ratio of water, hydrogen peroxide and ammonia solution are in the ratio 5:1:1. The substrates are then placed in the bubbling solution with the conducting side kept facing up. After 5-10 min of RCA treatment, the substrates are transferred to de-ionized water and sonicated for 5 min followed by blow-drying.

2.2.3 Fabrication of electron buffer layer (ZnO) thin film

20 µL of the original nano-dispersion solution (40 wt% of ZnO nanoparticles in ethanol) obtained from Sigma Aldrich is diluted with 980 µL of ethanol to make 1 mL of ZnO nanoparticle dispersion. The dispersion is then stirred at 65^{o}C for 30 minutes to achieve homogeneity. The solution is then cooled to room temperature and spin coated at 2000 rpm on the ITO coated glass slides. The substrates are then annealed at 120^{o}C for 60 minutes.

2.2.4 Fabrication of active layer thin film

PFO is mixed with $PC_{60}BM$ in 1:4 w/w ratio in 1,2 dichlorobenzene (DCB) at a concentration of 30 mg/ml. The solution was stirred overnight at 60^{o}C before use. The active layer is spin-coated on the ZnO buffer layer within a glove box environment (O_2 ~ 1 ppm, H_2O < 1 ppm) at 800 rpm. The coated substrates are annealed on a hot plate in the glove box environment at 60^{o}C for 1 hr.

2.2.5 Thermal Deposition

Hole buffer layer (molybdenum oxide) and the top electrode (silver) are coated by thermal deposition. MoOx was loaded on the boat and silver was loaded onto a basket. Physical masks of 4.5mm^2 active area were placed on the polymer layer and then put inside the evaporation chamber. The chamber containing the samples and required materials to be coated was evacuated using

rotary and turbo pump. Before evaporating the respective materials, their parameters like density and acoustic impedance are entered in film thickness monitor. When the pressure reaches $5*10^{-6}$ mbar, current is passed through the boat or the basket which evaporates the materials. The rate of coating is controlled by the current applied. A crystal oscillator-based thickness monitor was used to monitor the thickness of the material being coated. Initially, the rate of the coating was maintained at around 1 nm/s. The rate is increased as the coating proceeds. The samples are allowed to cool down for 2 hours after the coating is done. 9 nm of MoO_3 and 120 nm of Ag was coated on the polymer layer.

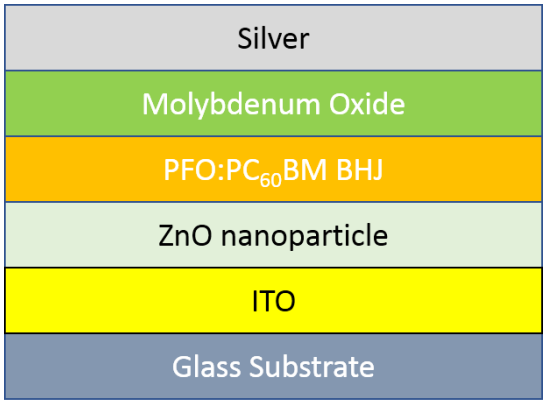

Figure 2.5: Device Structure of the binary blend photodiode

2.3 Characterisation of the PFO:PC_{60}BM photodiode

2.3.1 Current Density (J) – Voltage (V) measurement

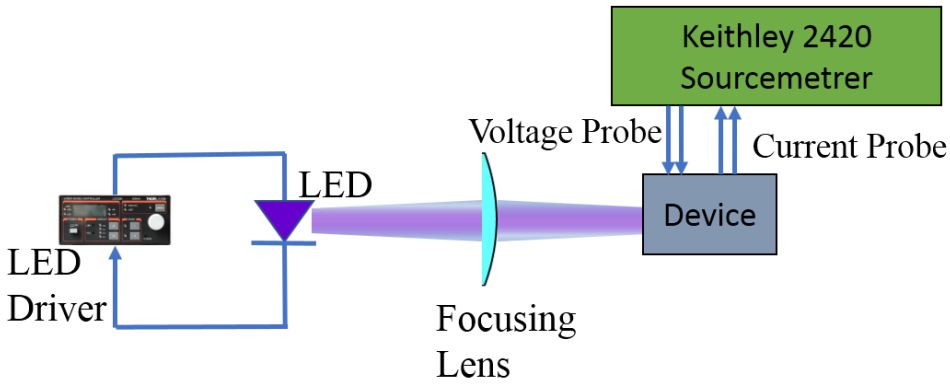

Figure 2.6: Experimental Set up for J-V characterization of the device

The J-V characterization of the photodiodes were done by sweeping the source voltage from 1.0 V to -0.4V with 200 sweep points between them. The experimental setup consists of Four-Probe configuration with two leads sweeping the voltage and other two leads measuring current. The voltage across the devices was applied and the current was measured using a Keithley 2420 Source

Meter interfaced with data acquisition software in the computer through LabView. The schematic diagram is given by figure 2.7. The J-V characterization of the samples were first done in dark conditions followed by illumination with 1 mW 405nm LED focused by a lens. Figure 2.8. shows the J-V diagram in dark as well as in illumination.

Very low dark currents were observed from the device in the range of 0.1 nA. The V_{oc} and J_{sc} obtained was 0.67 V and 0.39 µA/cm^2.

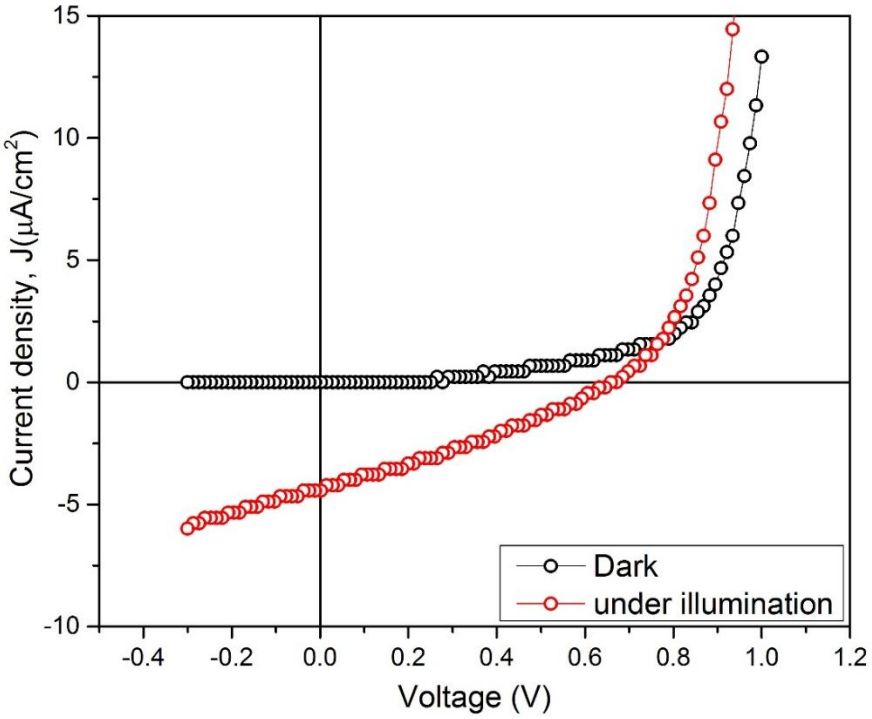

Figure 2.7: J-V curves of the binary blend device under dark and illuminated conditions

2.3.2 Responsivity

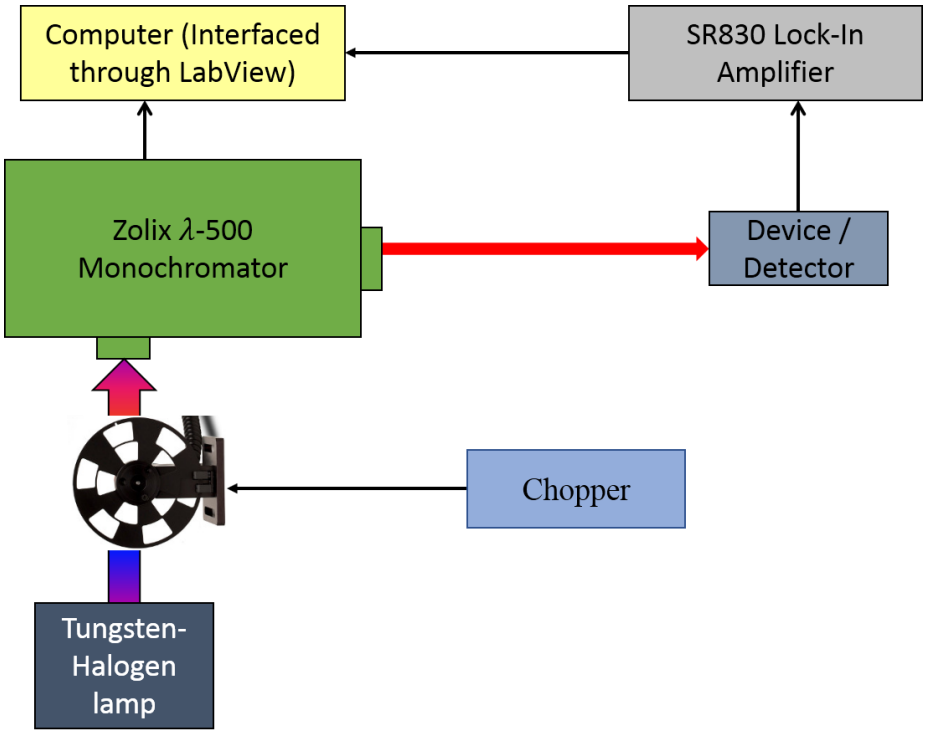

Figure 2.8: Experimental setup for obtaining responsivity spectra

Figure 2.9 shows the experimental setup to obtain responsivity as a function of wavelength. The experimental setup consists of a light source (Zolix LSH – T150 Tungsten Halogen Lamp) coupled with Zolix λ-500 monochromator. The width of output light from the monochromator is controlled through a slit and this was used to keep the illumination on the device or the calibration detector constant. Device was measured under short circuit condition. The current output was measured using Stanford Research Systems SR830 Lock-in Amplifier. The light from the source was modulated using a chopper at 287 Hz and this was used as reference frequency for the Lock -in amplifier. The time constant used for the Lock-in amplifier was 300 ms so that clean signals were obtained from the detectors. The monochromator and the Lock-in amplifier were interfaced with the computer using LabView. The power of the source was calibrated using a Zolix silicon detector and it was calculated by dividing J_{sc} of the detector at each wavelength by the corresponding responsivity (A/W) of the detector at each of the wavelength. Area normalization was done by keeping the detector in the same place as the device. Photocurrent spectra scan was done by sweeping the wavelength between 350 nm to 750 nm, with steps of 1nm. Time delay at each step is kept at one second. The current output from the detector was divided by the source power to obtain the responsivity.

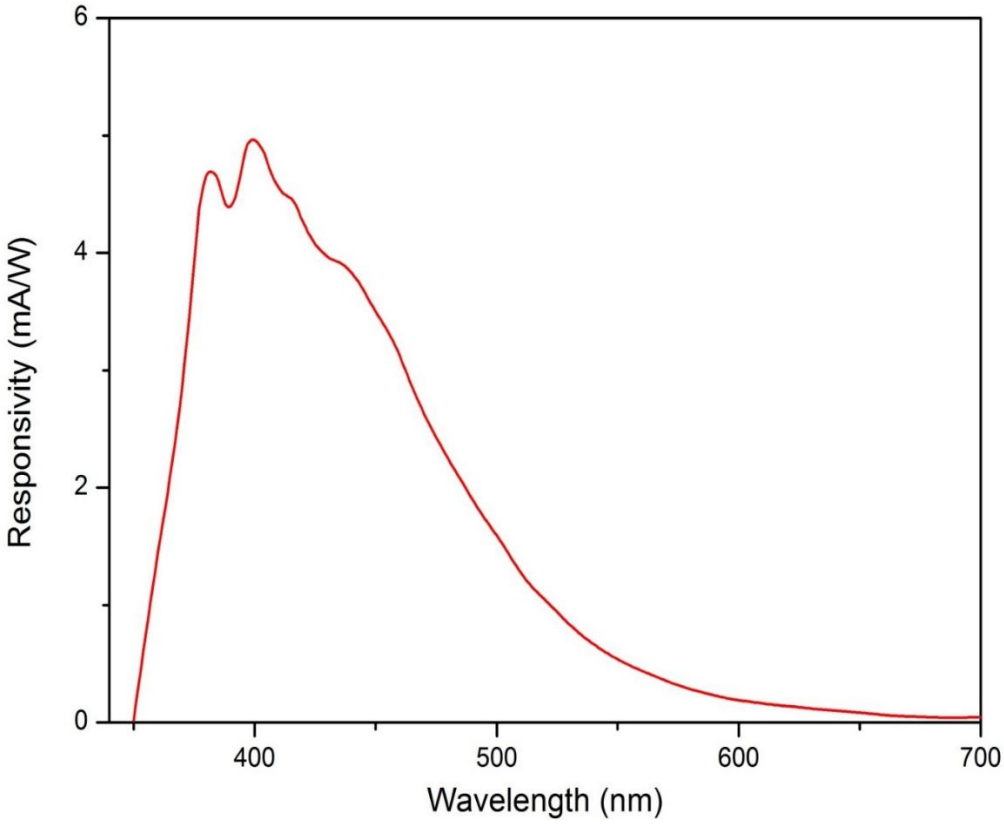

Figure 2.9: Responsivity spectrum of the device

The Responsivity vs the wavelength curve of the device (Figure 2.10) shows that the device has very less overlap with the emission spectra of the yellow phosphor with significantly high responsivity in region of GaN emission spectra.

2.3.3 Frequency Response

A normal off the shelf 405nm LED was focused using a convex lens on the OPD. The LED was driven by Thor Labs LDC500 laser diode controller. Sinusoidal modulation of various frequencies with an amplitude of 5 V was fed to the LED from the AFG output of Tektronix MDO3024 200 MHz oscilloscope. This was fed to the RF input of the driver. The LDC 500 Laser Diode controller is basically a bias tee circuit. A bias tee is a circuit which consists of a parallel combination of an ideal inductor which allows DC bias through and blocks any RF signal and an ideal capacitor at which vice versa happens. The voltage signals then get added up to give rise to an amplitude modulation of the LED. The device is operated in short circuit condition. The OPD signal waveform and the modulated LED signal were obtained and compared using a Tektronix 200 MHz Mixed Domain Oscilloscope at AC 1 MΩ coupling. Figure 2.11 gives a schematic of the experiment. The OPD shows good response at 400 kHz as shown in Fig 2.12.

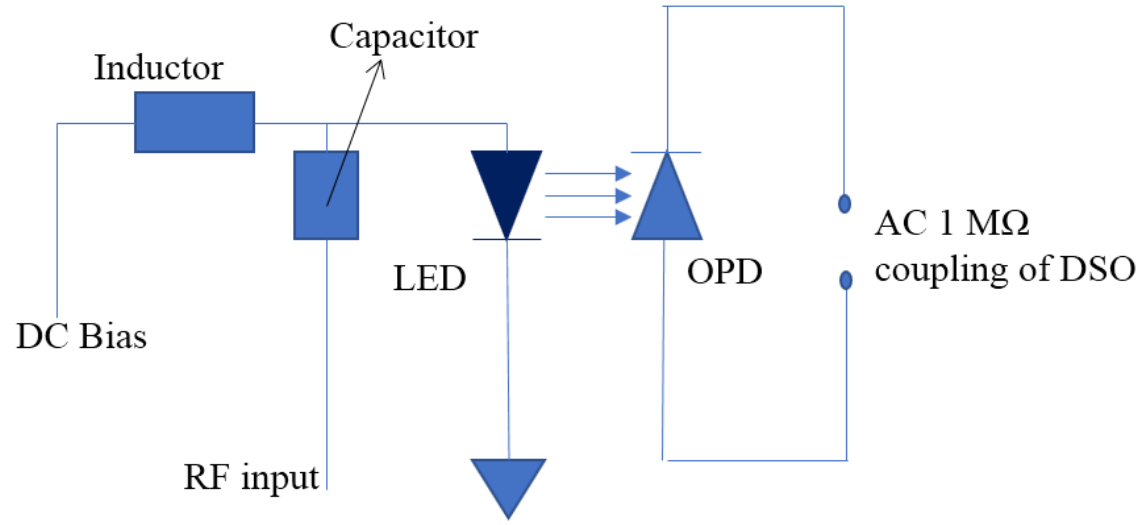

Figure 2.10: Experimental set up for frequency response of the device

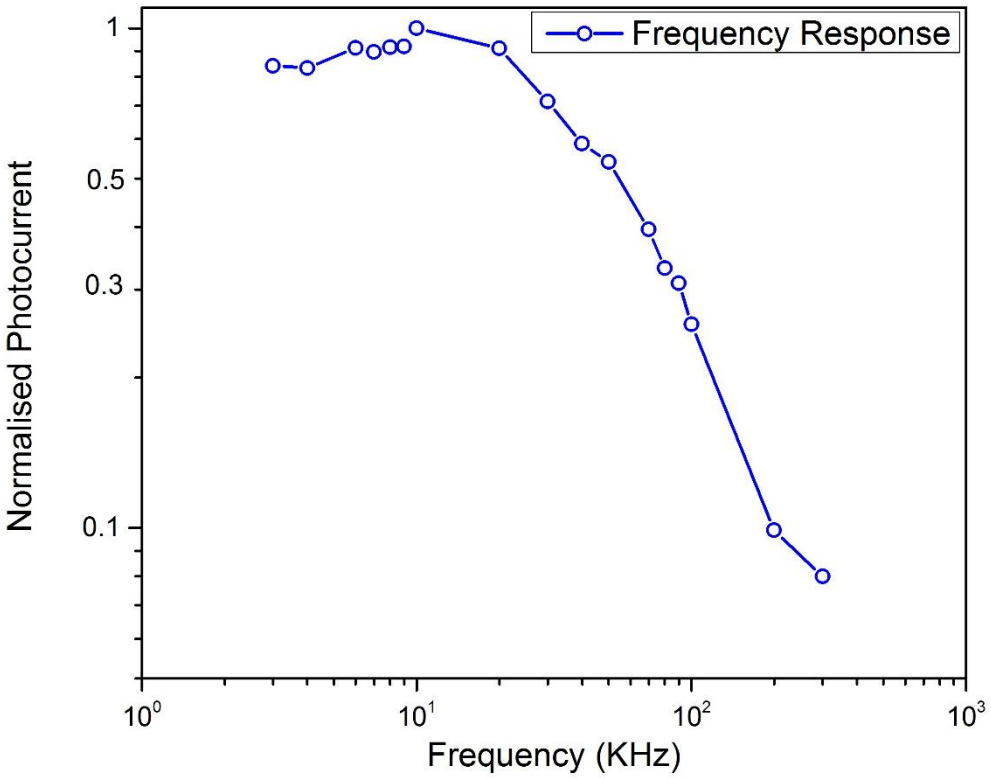

Figure 2.11: Frequency response of the device

2.3.4 Intensity vs photocurrent curve

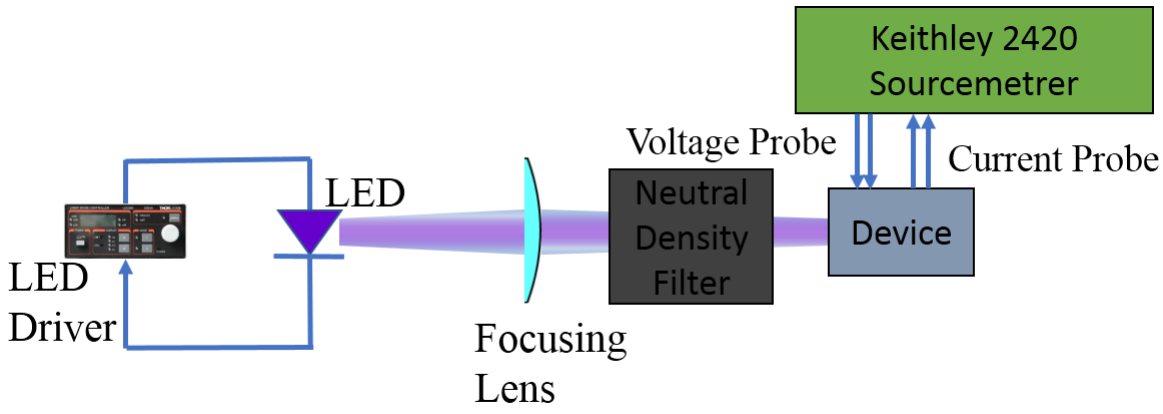

Figure 2.12: Experimental setup for measuring intensity versus photocurrent

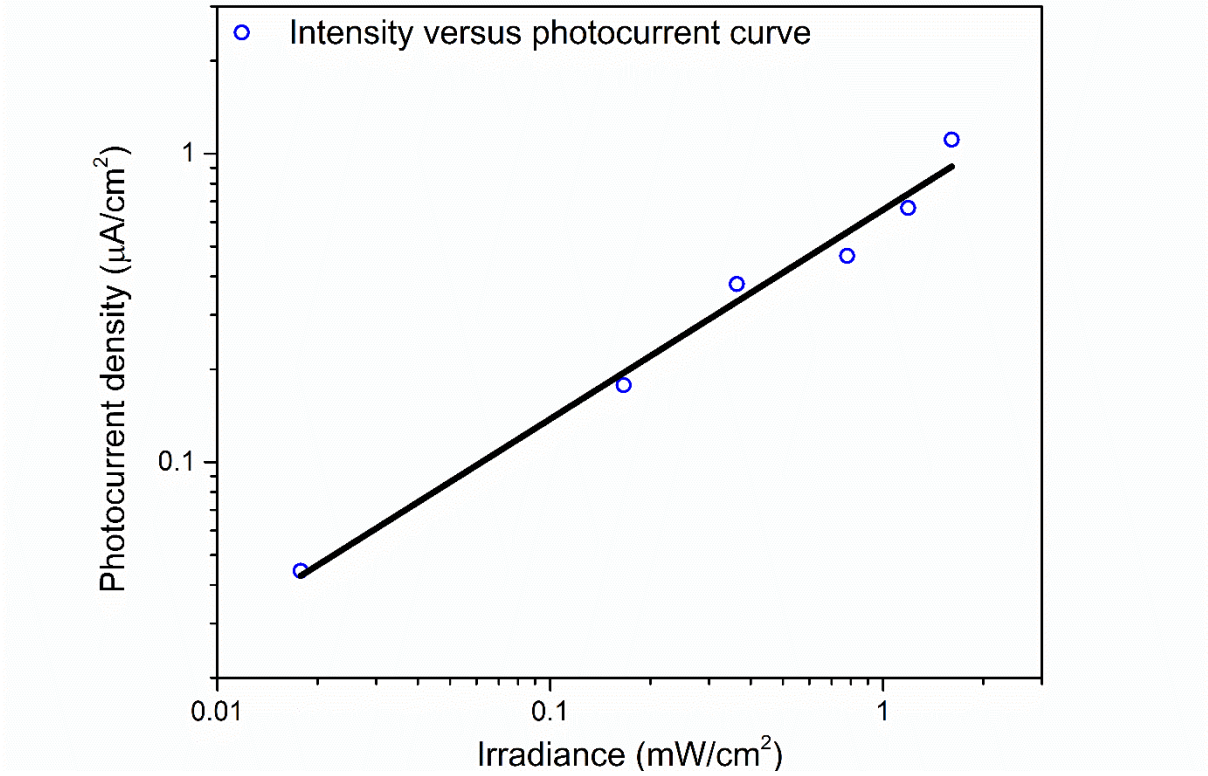

Figure 2.13: Irradiance versus photocurrent curve

The photocurrent versus the intensity of light was obtained by doing J-V scans under different levels of illumination. A 405 nm LED was driven by Thor Labs LDC500 Laser Diode Controller. The LED light was focused using a convex lens on the device. Between the lens and the device neutral density filters were kept to vary the intensity of the LED light. The highest illumination that was focused on the sample was 2 mW. A schematic diagram is shown in Fig 2.14.

2.4 Discussion

Very low dark currents were observed from the device in the range of 0.1 nA. The responsivity curve of the PFO:$PC_{60}BM$ devices indicates that its overlap between the emission spectra of the slow yellow phosphor component in the white LED has been significantly decreased. The spectral range of the photodiode was 370nm to 520 nm with high responsivity of greater than 1 mA/W. The highest responsivity was observed to be ~5 mA/W at around 440 nm. The irradiance versus the photocurrent curve is linear over two orders of intensity.

A clear response of the binary blend polymer photodiode was seen up-to 0.4 MHz which asserts that this class of devices are strong candidates for exhibiting high-speed photodetection. The speed of the OPD is mainly limited by the mobility of the polymer which is ~ 10^{-3} $cm^2/V.s$[14]. Also, the thickness of the device (which is basically the addition of all the dielectric layers in the device) increases the transit time of carriers in the device leading to a limitation in its speed.

2.5 References

1 Chunwaschirasiri, W., Tanto, B., Huber, D. & Winokur, M. Chain conformations and photoluminescence of poly (di-n-octylfluorene). *Physical review letters* **94**, 107402 (2005).

2 Guha, S., Chandrasekhar, M., Scherf, U. & Knaapila, M. Tuning structural and optical properties of blue-emitting polymeric semiconductors. *physica status solidi (b)* **248**, 1083-1090 (2011).

3 Campbell, A. J., Bradley, D. D. & Antoniadis, H. Dispersive electron transport in an electroluminescent polyfluorene copolymer measured by the current integration time-of-flight method. *Applied Physics Letters* **79**, 2133-2135 (2001).

4 Ahn, J. H., Wang, C., Perepichka, I. F., Bryce, M. R. & Petty, M. C. Blue organic light emitting devices with improved color purity and efficiency through blending of poly (9, 9-dioctyl-2, 7-fluorene) with an electron transporting material. *Journal of Materials Chemistry* **17**, 2996-3001 (2007).

5 Gross, M. *et al.* Improving the performance of doped [pi]-conjugated polymers for use in organic light-emitting diodes. *Nature* **405**, 661-665 (2000).

6 Ohmori, Y., Hamasaki, T., Morimune, T. & Kajii, H. in *Photonics Europe.* 69990W-69990W-69998 (International Society for Optics and Photonics).

7 Zhang, F. *et al.* Influence of PC60BM or PC70BM as electron acceptor on the performance of polymer solar cells. *Solar Energy Materials and Solar Cells* **97**, 71-77, doi:http://dx.doi.org/10.1016/j.solmat.2011.09.006 (2012).

8 Roncali, J. Linear [small pi]-conjugated systems derivatized with C60-fullerene as molecular heterojunctions for organic photovoltaics. *Chemical Society Reviews* **34**, 483-495, doi:10.1039/b415941c (2005).

9 Zhao, J. *et al.* Phase Diagram of P3HT/PCBM Blends and Its Implication for the Stability of Morphology. *The Journal of Physical Chemistry B* **113**, 1587-1591, doi:10.1021/jp804151a (2009).

10 Po, R., Carbonera, C., Bernardi, A. & Camaioni, N. The role of buffer layers in polymer solar cells. *Energy & Environmental Science* **4**, 285-310, doi:10.1039/c0ee00273a (2011).

11 Tao, C. *et al.* Performance improvement of inverted polymer solar cells with different top electrodes by introducing a MoO3 buffer layer. *Applied Physics Letters* **93**, -, doi:doi:http://dx.doi.org/10.1063/1.3026741 (2008).

12 Yamanari, T., Taima, T., Sakai, J., Tsukamoto, J. & Yoshida, Y. Effect of Buffer Layers on Stability of Polymer-Based Organic Solar Cells. *Japanese Journal of Applied Physics* **49**, 01AC02.

13 White, M. S., Olson, D. C., Shaheen, S. E., Kopidakis, N. & Ginley, D. S. Inverted bulk-heterojunction organic photovoltaic device using a solution-derived ZnO underlayer. *Applied Physics Letters* **89**, -, doi:doi:http://dx.doi.org/10.1063/1.2359579 (2006).

14 Babel, A. & Jenekhe, S. A. Charge Carrier Mobility in Blends of Poly(9,9-dioctylfluorene) and Poly(3-hexylthiophene). *Macromolecules* **36**, 7759-7764, doi:10.1021/ma034717t (2003).

CHAPTER 2

CHAPTER 3

CHARACTERISTICS OF TERNARY BLEND BHJ PHOTODIODES

In the last chapter, a blue sensitive photodiode was fabricated that had a temporal response up to 0.4 MHz. To enhance the temporal response and responsivity in the NIR region, a squaraine derivative was blended with poly(9,9-dioctylfluorenyl-2,7-diyl) (PFO) and [6-6]phenyl-C61-butyric acid methylester (PCBM) to form a ternary blend. This chapter deals with the fabrication protocols and characterization of this photodiode fabricated from this ternary blend.

3.1 Materials

3.1.1 Donor Molecules

Poly(9,9-dioctylfluorene-2,7-diyl) (PFO) with a band-gap of 3.2 eV and an absorption maximum at 390 nm is one of the ideal contenders for optical communication. It has a very narrow absorption range from 330 nm to 460 nm. The PFO used for device fabrication was bought from Luminescent Technologies, Taiwan.

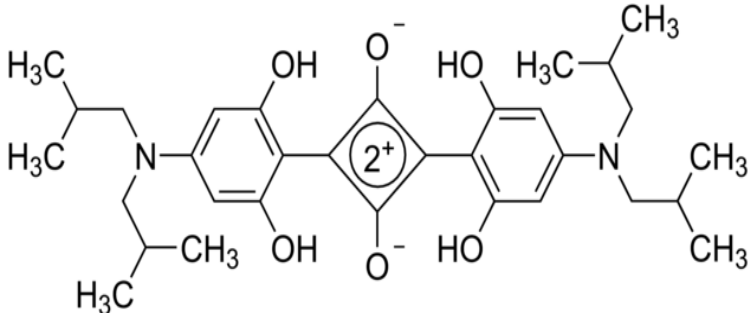

Figure 3.1 Structure of DPSQ

Squaraines are a class of small molecular zwitterionic organic dyes which are generally prepared by the condensation of electron-rich aromatic or heterocyclic compounds such as benzothiazoles, N,N-dialkylanilines, phenols, azulenes, and pryrroles with squaric acid[1]. The small molecules are advantageous because they are intrinsically mono-dispersive, band gap tunable, easy to synthesize and purify[2,3] compared to polymers. Synthesis of various electron rich aromatic and heterocyclic systems that react with squaric acid leads to its tunable optical properties. The optical absorption of the squaraines are generally red shifted either by using strong electron donors or by the

extension of conjugation i.e by changing the length of the alkyl chain[1].The squaraine molecules are widely used in different applications such as imaging[4], sensing[1] and photovoltaics[5-11]. The squaraine molecules are highly stable with a large absorption coefficient ($\alpha \sim 3 \times 10^5$ cm^{-1}) [12]. Apart from PFO, DP squaraine (DPSQ) is used as the donor which is utilized for its very narrow spectral range from 625 nm to 725 nm.

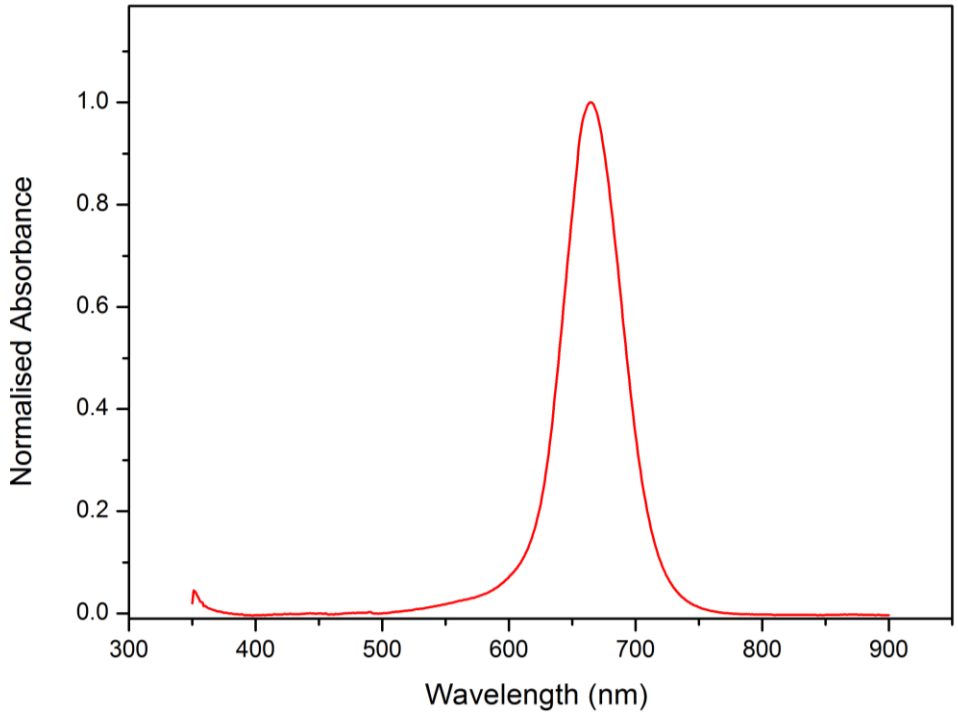

Figure 3.2: Absorption spectrum of DPSQ

3.1.2 Acceptor Molecule

As mentioned in the previous chapter, [6,6]-phenyl-C_{61}-butyric acid methyl ester ($PC_{60}BM$) obtained from Luminescent Technologies, Taiwan was used as an acceptor. The molecule absorbs in the wavelength range of 200 nm to 400 nm with absorption maximum around 270 nm.

3.1.3 Buffer Layers and Electrodes

The hole buffer layer used in the fabrication of the ternary blend is Molybdenum oxide with a HOMO of around -5.3 eV and LUMO of around -2.4 eV. Zinc oxide nanoparticles (NP) were used as the electron buffer layer with HOMO of -7.5 eV and LUMO of -4.1 eV. Indium Tin Oxide (ITO) was used as the electron collecting electrode and silver as the hole collecting electrode. The work functions of ITO and silver are -4.7 eV and -4.73 eV respectively.

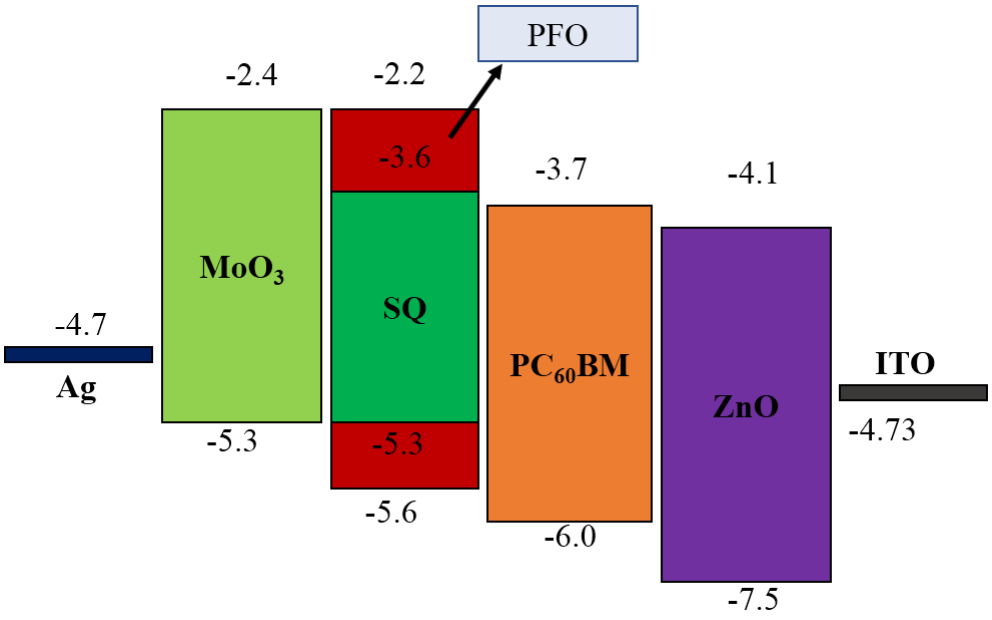

Figure 3.3: Energy level diagram of the layers used in the device

3.2 Photodiode Fabrication

PFO:DPSQ:$PC_{60}BM$ photodiode used in our experiments were fabricated in inverted solar cell geometry. Since DPSQ does not have a very good solubility with 1,2 dichlorobenzene, the films formed from the blend initially were discontinuous. So, various solvents were tried to see in which solvent DPSQ gives better films. It was observed that chloroform is the ideal solvent[13] for getting better films of DPSQ. But the main problem with chloroform was that it had a very low boiling point and so it was not very ideal for device fabrication. Thus, the ternary blend solution of PFO, $PC_{60}BM$ and DPSQ was made in 1:1 volume by volume ratio with 1,2 dichlorobenzene. The presence of 1,2 dichlorobenzene elevates the boiling point of the solvent thus giving better films. The ternary blend solution was left stirring overnight at 65ºC.

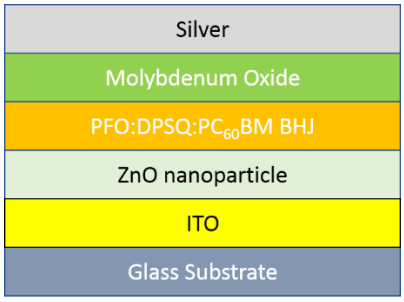

Figure 3.4: Device structure of the ternary blend BHJ photodiode

The ITO substrates were masked and etched using HCl and Zn dust. They were thoroughly washed with de-ionized water after etching. Afterward, the slides were first cleaned with Extran, then with

IPA and acetone solution followed by RCA cleaning as described in the last chapter. The RCA cleaned sample was spin coated with ZnO NP at 2000 rpm and then annealed at 120ºC for an hour.

The hot solution containing the active layer was spin coated at 900 rpm. This was then annealed at 65ºC for one hour. On this active layer, physical masks were put and MoO and silver were thermally evaporated sequentially at 5 x 10^{-6} mbar of pressure. The thickness of MoO coated was around 9 nm and the thickness of silver coated was around 120 nm.

3.3 Characterisation of the photodiode

3.3.1 Current Density (J) – Voltage (V) measurement

The J-V characterization of the photodiodes was done by sweeping the source voltage from 1.0 V to -0.4V with 200 sweep points between them.

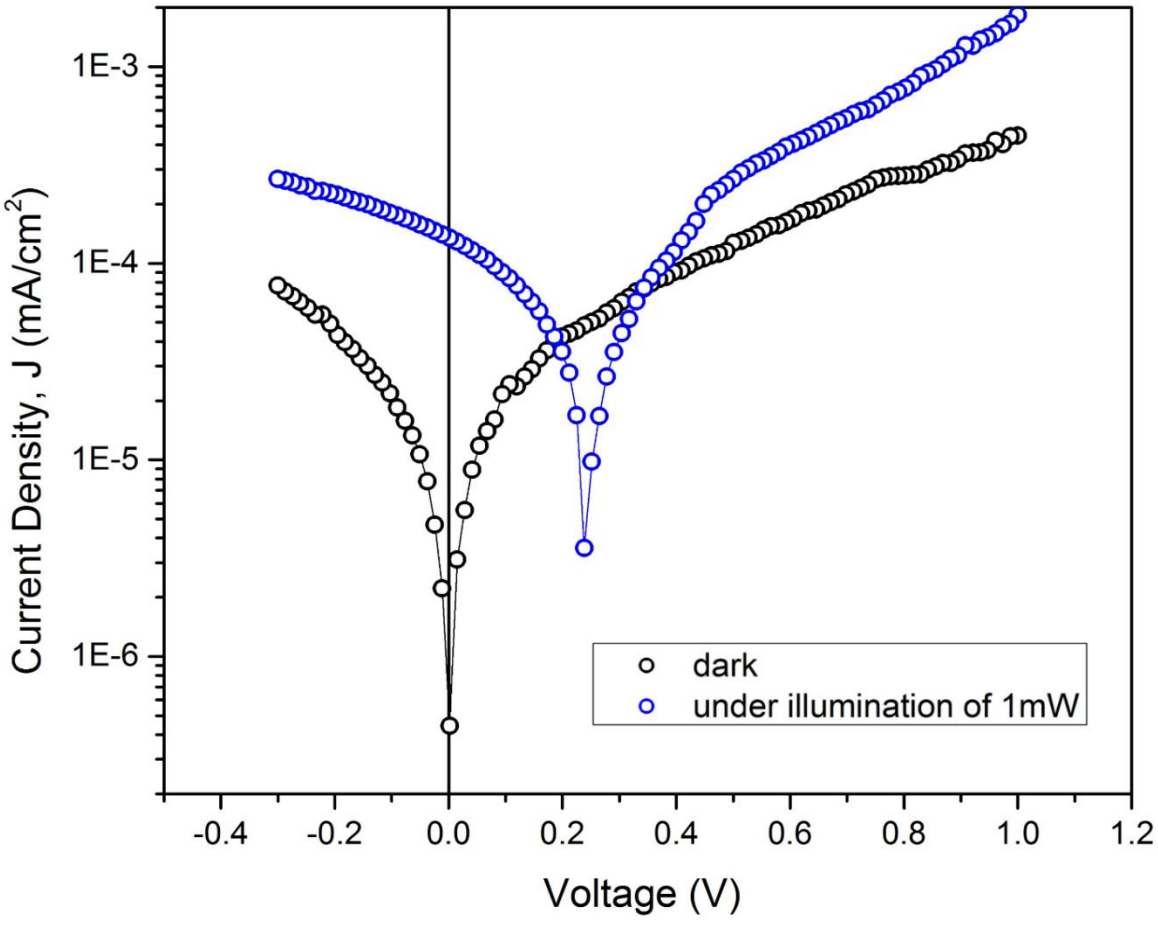

Figure 3.5: J-V characteristics of the device under dark and illumination

The experimental setup consists of Four-Probe configuration with two leads sweeping the voltage and other two leads measuring current. The voltage across the devices was applied using a Keithley 2420 Source Meter interfaced with data acquisition software in the computer using LabView. The

schematic diagram is given by figure 2.7. The J-V characterization of the samples was first done in dark conditions followed by illumination with 1 mW 405 nm LED focused by a lens. Figure 3.5 shows the J-V characteristics in dark as well as in illumination. Dark currents in the range of 1 µA were observed from the photodiode.

3.3.2 Responsivity

The experimental setup consists of a light source (Zolix LSH – T150 Tungsten Halogen Lamp) coupled with Zolix λ-500 monochromator. Device was measured under short circuit condition. The current output was measured using Stanford Research Systems SR830 Lock-in Amplifier. The light from the source was modulated using a chopper at 281 Hz and this was used as the reference frequency for the Lock-in amplifier. The time constant used for the Lock-in amplifier was 300 ms so that clean signals were obtained from the detectors. The monochromator and the Lock-in amplifier were interfaced with the computer using LabView. Area normalization was done by keeping the detector in the same place as the device. Photocurrent spectra scan was done by sweeping the wavelength between 350 nm to 850 nm, with steps of 1nm. Time delay at each step was kept at one second. The current output from the detector was divided by the source power to obtain the responsivity. The schematic diagram is shown in figure 2.9.

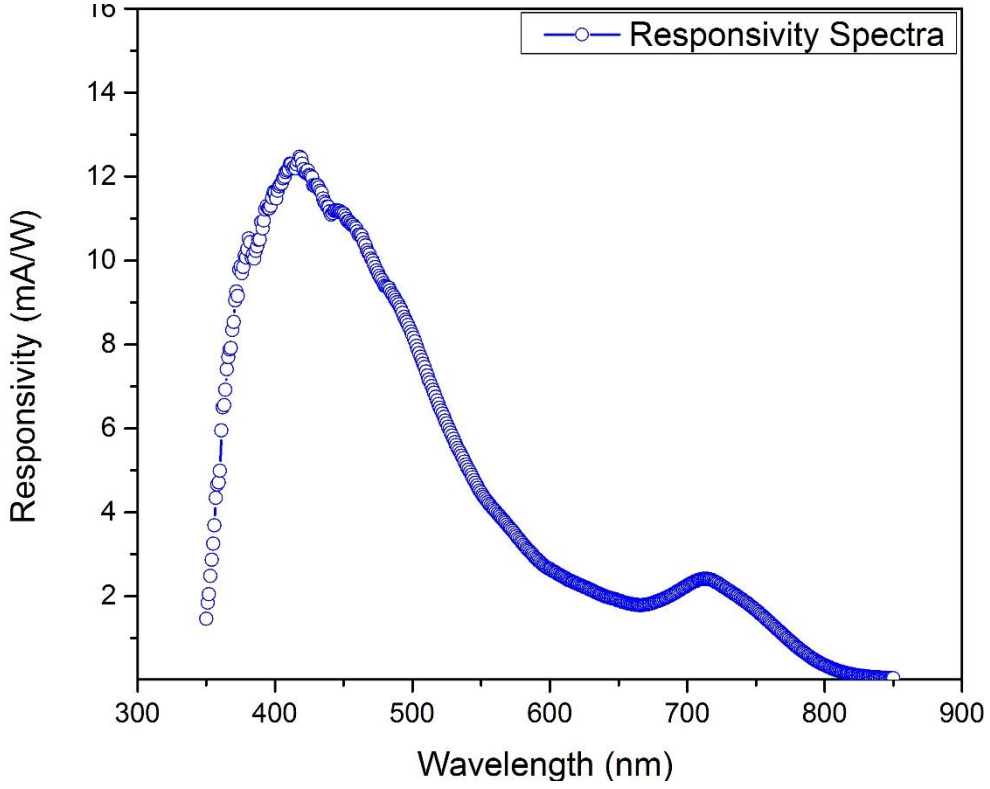

Figure 3.6: Responsivity spectrum of the device

3.3.3 Frequency Response

A normal off the shelf 405nm LED was focused using a convex lens on the OPD. The LED was driven by Thor Labs LDC500 laser diode controller. Sinusoidal modulation of various frequencies with an amplitude of 5 V was fed to the LED from the AFG output of Tektronix MDO3024 200 MHz oscilloscope. This was fed to the RF input of the driver which is basically a bias tee circuit. The bias tee gives rise to intensity amplitude modulation of the LED. The device was operated in short circuit condition. The OPD signal waveform and the modulated LED signal was read and compared using a Tektronix 200 MHz Mixed Domain Oscilloscope at AC 1 MΩ coupling. Figure 2.11 gives schematic of the experiment.

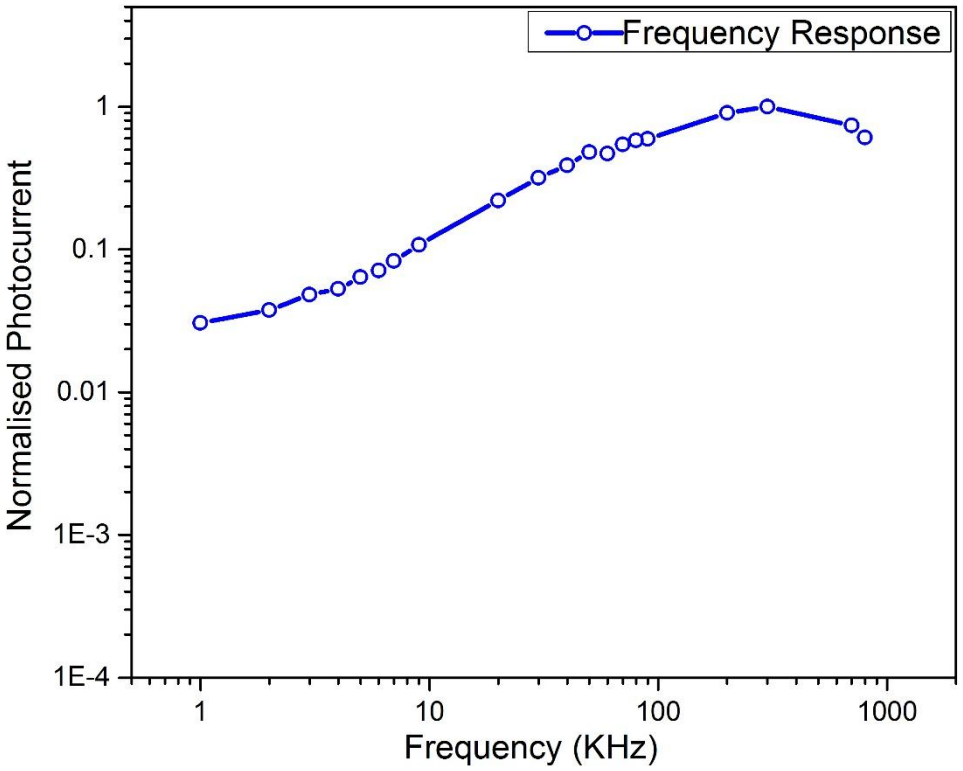

Figure 3.7: Frequency response of the device

3.3.4 Intensity Dependence

The photocurrent versus the intensity of light was obtained by doing J-V scans under different levels of illumination. A 405 nm LED was driven by Thor Labs LDC500 Laser Diode Controller. The LED light was focused using a convex lens on the device. Between the lens and the device, neutral density filters were kept to vary the intensity of the LED light. The highest illumination that was focused on the sample was 2 mW. The schematic diagram is shown in Fig 2.13

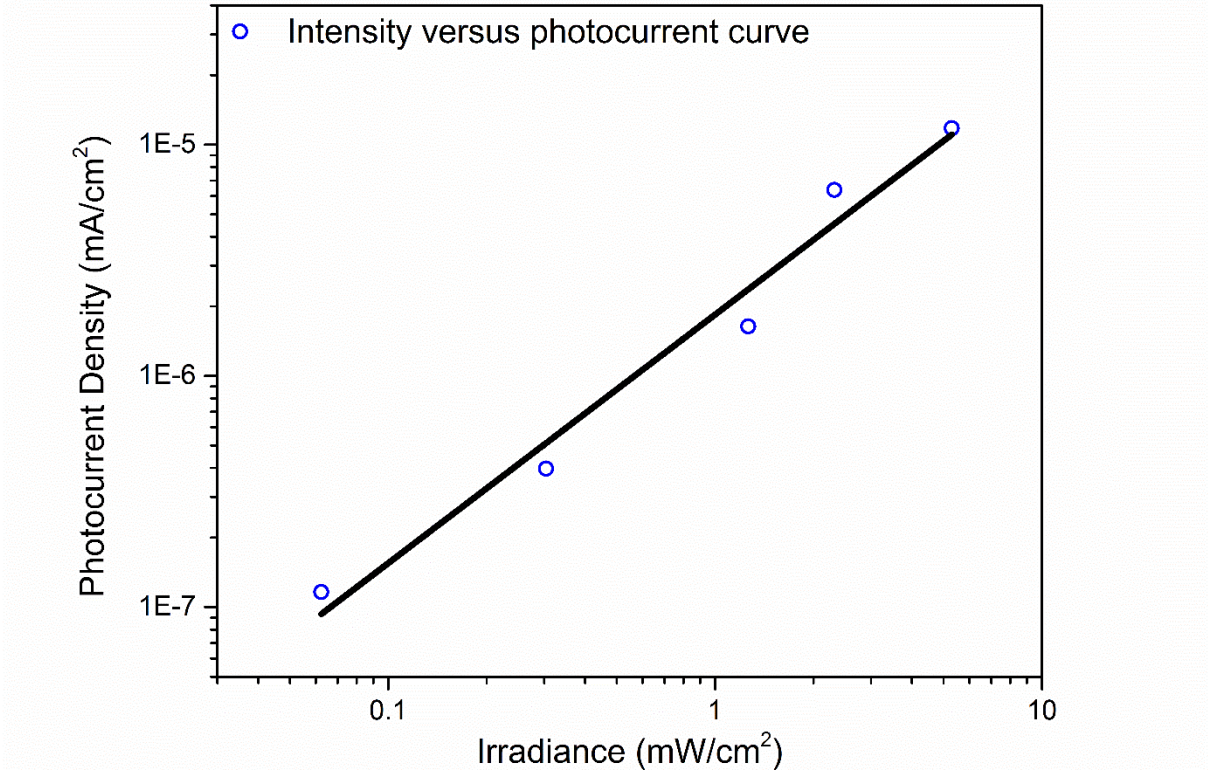

Figure 3.8: Irradiance versus photocurrent density of the device

3.4 Discussion

The responsivity curve of the ternary blend devices indicates that the addition of DPSQ in the PFO:$PC_{60}BM$ system enhances its responsivity. The spectral range of the photodiode was 370nm to 820 nm with high responsivity of greater than 1 mA/W. The with highest responsivity was ~13 mA/W at around 440 nm. The irradiance versus the photocurrent curve is linear over three orders of intensity.

A clear response of the binary blend polymer photodiode was seen beyond 0.8 MHz which asserts that this class of devices are strong candidates for exhibiting high-speed photodetection. Thus, the addition of DPSQ to the binary blend photodiode increased both the bandwidth and responsivity of the photodiode. A clear response of the ternary blend polymer photodiode was seen beyond 0.8 MHz which asserts that this class of devices can be used in applications which require high-speed photodetection both in the blue and in the NIR region.

3.5 References

1 Ajayaghosh, A. Chemistry of squaraine-derived materials: near-IR dyes, low band gap systems, and cation sensors. *Accounts of Chemical Research* **38**, 449-459 (2005).

2 Walker, B., Kim, C. & Nguyen, T.-Q. Small molecule solution-processed bulk heterojunction solar cells. *Chemistry of Materials* **23**, 470-482 (2010).

3 Roncali, J. Molecular bulk heterojunctions: an emerging approach to organic solar cells. *Accounts of chemical research* **42**, 1719-1730 (2009).

4 Tam, A. Optoacoustic determination of photocarrier generation efficiencies of dye films. *Applied Physics Letters* **37**, 978-981 (1980).

5 Velez, M., Zyss, J., Ledoux, I. & Chengg, L.-T. Squarylium dyes: structural factors pertaining to the negative third-order nonlinear optical response. *J. Am. Chem. Soc* **117**, 2214-2225 (1995).

6 Ashwell, G., Jefferies, G., Hamilton, D. & Lynch, D. Strong second-harmonic generation from centrosymmetric dyes. *Nature* **375**, 385 (1995).

7 Varma, P. R. & Namboothiry, M. A. Squaraine based solution processed inverted bulk heterojunction solar cells processed in air. *Physical Chemistry Chemical Physics* **18**, 3438-3443 (2016).

8 Rao, G. H. *et al.* Near-infrared squaraine co-sensitizer for high-efficiency dye-sensitized solar cells. *Physical Chemistry Chemical Physics* **18**, 14279-14285 (2016).

9 Yan, Z., Guang, S., Su, X. & Xu, H. Near-infrared absorbing squaraine dyes for solar cells: relationship between architecture and performance. *The Journal of Physical Chemistry C* **116**, 8894-8900 (2012).

10 Chang, C.-H., Chen, Y.-C., Hsu, C.-Y., Chou, H.-H. & Lin, J. T. Squaraine-arylamine sensitizers for highly efficient p-type dye-sensitized solar cells. *Organic letters* **14**, 4726-4729 (2012).

11 Wang, S. *et al.* High efficiency organic photovoltaic cells based on a vapor deposited squaraine donor. *Applied Physics Letters* **94**, 156 (2009).

12 Chen, G. *et al.* Optical and electrical properties of a squaraine dye in photovoltaic cells. *Applied Physics Letters* **101**, 083904 (2012).

13 Sasabe, H. *et al.* Soluble squaraine derivatives for 4.9% efficient organic photovoltaic cells. *RSC Advances* **4**, 42804-42807 (2014).

CHAPTER 3

CHAPTER 3

CHAPTER 4

Effect Of Non-Line Of Sight Luminescent Emitters in Visible Light Communication Systems

Optical communication technology prevails in the presence of a background lighting condition. Thus, strategies to mitigate ambient light effects in VLC systems have been implemented both in the communication hardware and signal processing stages [1-3]. Blue LEDs which employ phosphor converters to generate white light now employ color converters with lifetimes much lesser than the phosphor [4], thus leading to bandwidth improvements. In the scheme of internet-of-things, the wall features such as texture, color, reflectance, glow etc. , can assume significant importance. The enclosure boundary is normally treated as a classical light diffuser which merely scatters and attenuates the signal [1, 2]. The use of these external emitters as active noise sources can distort the signal and alter the communication characteristics [8-10]. The introduction of active contributions which can alter the source-generated signal features, or more specifically the noise characteristics forms the central theme of this chapter.

4.1 Noise in Photodetectors

The noise observed in photodiodes show different features in the frequency domain. Based on their features they are categorized as follows:

Thermal Noise

Thermal Noise (also called Nyquist noise or Johnson noise) arises due to thermal agitation of charge carriers (which gets reflected on to the resistance) in the device. The voltage power spectral density (PSD) (V^2/Hz) is given by

$$S_V(f) = 4K_BTR \qquad (4\text{-}1)$$

Similarly, the current PSD (A^2/Hz) is given by

$$S_I(f) = 4K_BT/R \qquad (4\text{-}2)$$

where K_B is the Boltzmann constant, T is the absolute temperature, R is the resistance. Thermal noise is independent of frequency i. e. , its spectrum is white in nature. Thermal noise doesn't distinguish between materials as long as the resistance value is the same.

Shot Noise

Shot noise in a photodiode arises due to the quantization of charge carriers and is also white in nature. Shot noise generally dominates when the number of charge carriers are low so that the quantization of charge carriers is clearly evident. The spectral power is given as

$$S_I(f) = 2eI \qquad (4\text{-}3)$$

Where e is the electronic charge and I is the current. Shot noise is observed at low temperatures where the thermal noise does not dominate.

Flicker noise ($1/f$ noise)

Flicker noise has been the center of attention in the last few decades because it represents the quality or reliability of a device. As the name suggests its magnitude is inversely proportional to the frequency that is it has a $1/f$ dependence. This noise in semiconductor was modelled by Hooge and the power spectral density is given as

$$S_I(f) = \frac{\alpha_H}{fN} I^2 \qquad (4\text{-}4)$$

Where α_H is the Hooge's parameter, N is the number of carriers, I is the current

Generally, in a semiconductor device, there are two kinds of fluctuation: (1) Fluctuation in the mobility of the device and (2) Fluctuation in the mobilities of carriers. Hooge's equation holds very well for mobility fluctuation. However, the origin of flicker noise is still debatable in the scientific community.

Generation-Recombination Noise

Generation-Recombination (g-r) noise in semiconductors is mainly contributed from the trapping and detrapping in the number of charge carriers which gives rise to their fluctuation in current transport. Traps states in semiconductors are generally electronic states in the forbidden band gap arising due to various defects and impurities in the bulk and at the surface or the interface. The PSD of g-r fluctuation is

$$S_N(f) = 4(\Delta N)^2 \frac{\tau}{1+2\pi f\tau} \qquad (4\text{-}5)$$

where τ is the time constant for transitions.

4.2 Photon noise detection

An array of avalanche photodiodes (APD) in the form of a photomultiplier module that has the ability to measure single photons is commonly used to study photon number fluctuations of light sources. The avalanche photodiodes in the array have their own sources of noise arising from intrinsic processes like fluctuations in the number and the positions at which the dark pairs are generated, apart from the statistical fluctuations of the incident photon flux contributing to the electron-hole generation[11]. In the APD, the process of internal photocurrent multiplication at sufficient reverse bias is used to achieve high sensitivity and is accompanied by excess noise during the multiplication [11]. The APD arrays can be further operated in photon-counting (Geiger mode) mode which can capture single photon fluctuations in the light sources for a fixed time interval. However, the APD arrays suffer from drawbacks of high thermal noise at high frequencies and optical crosstalk (emission of secondary photons in the array after one APD detects a photon due to hot carrier relaxation). Each of these sources can be modeled, identified and quantified by systematic noise measurement studies as a function of external parameters (light intensity, temperature, bias) and material parameters (mobility, trap density) [12, 13].

The capture of photon number fluctuation by the APD array involves three independent stochastic events [14]. Firstly, the charge carriers responsible for the driving current follow a noise distribution which gets reflected in the intensity fluctuation of the LED. The magnitude by which this fluctuation is transferred to the LED depends on the quantum efficiency of the LED (η_{LED}). Secondly, the emitted light from LED spreads over a large solid angle and even after various focusing mechanisms, a part of it gets lost before getting detected by the APD array. The efficiency with which the photon gets transferred from the LED to the detector is given by $\eta_{tranfer}$. The APD array has very high quantum efficiency (η_{APD}) and converts this stream of photons into photocurrent which captures the noise distribution of the light source. Thus, the net efficiency with which the whole process of noise can be captured is given as

$$\eta = \eta_{LED}\eta_{tranfer}\eta_{APD} \tag{4-6}$$

However, the individual efficiencies cannot be measured directly. The variance in the currents across the LED and APD array is the measurable quantity and is defined as

$$\Delta^2 i = < i^2 > - < i >^2 \tag{4-7}$$

These fluctuations are then normalized with respect to their mean currents and their ratio gives the extent by which the fluctuations of photons emitted from a source is captured by the APD.

4.3 Phosphorescence and Fluorescence

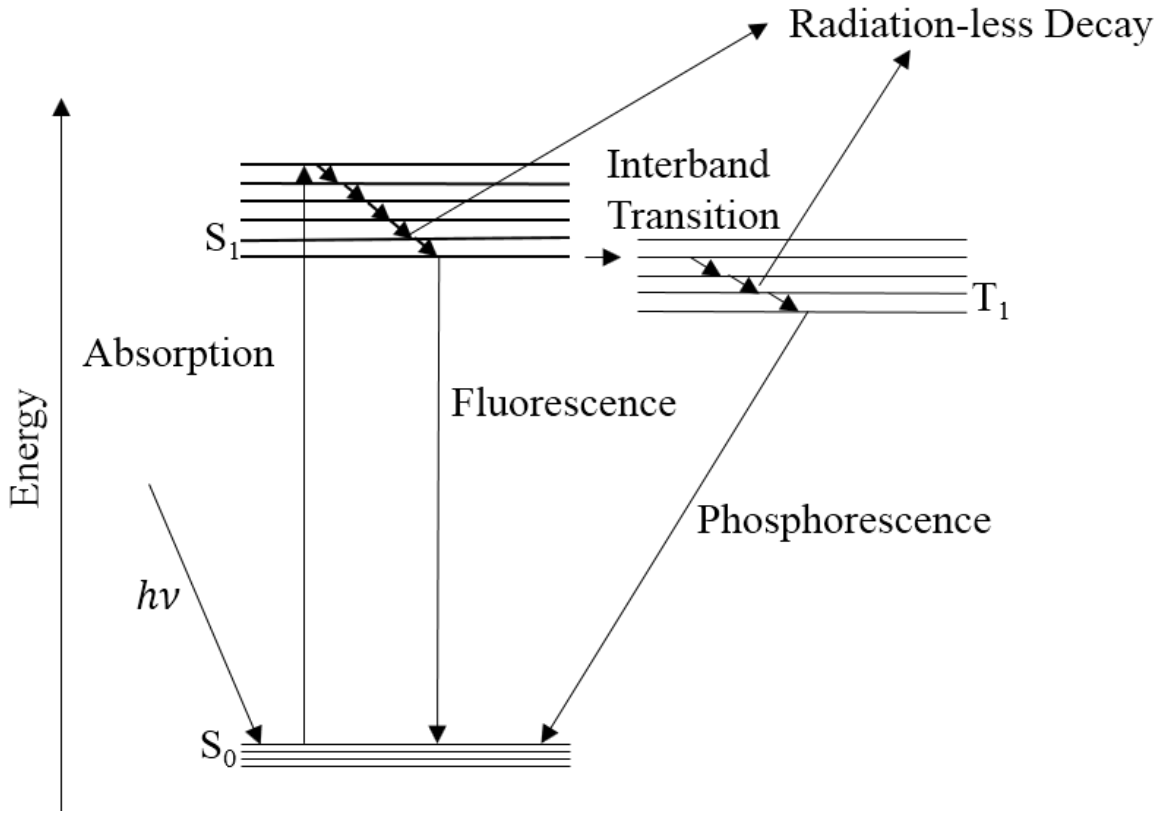

Figure 4.1: Jablonski Energy Diagram For A Photoluminescence system

Phosphorescence is a slow quantum process, involving at least three electronic states. The light from a pump source (in this case the LED) excites electrons to the excited singlet state (S_1) from the ground state (S_0). The electrons then undergo intersystem crossing and reach the triplet (T_1) state via a vibrational coupling. Since the transition from triplet to the singlet state is spin forbidden, the lifetime of the triplet state is quite larger which contributes to large lifetimes in the phosphorescent materials.

Fluorescence is the excitation of electrons from S_0 to S_1 which then undergo radiation-less decay to the lowest vibrational level of S_1 before getting deexcited to the S_0 state.

The presence of these phosphorescent emitters as paint on walls and boundaries play a significant role in changing the noise distribution of photons coming from the LED which will be shown in the later sections. These coatings can also be expected to play a sizable role in the bandwidth and the quality of the signal. A wide variety of coating attributes can be used as a parameter to provide spatial locations, where the detector signals can vary in strength. This strategy of a spatially selective signal distortion scheme involves phosphor based coatings and paints which provide a unique handle to create different levels of a smart environment.

4.4 Demonstration of NLOS communication setup

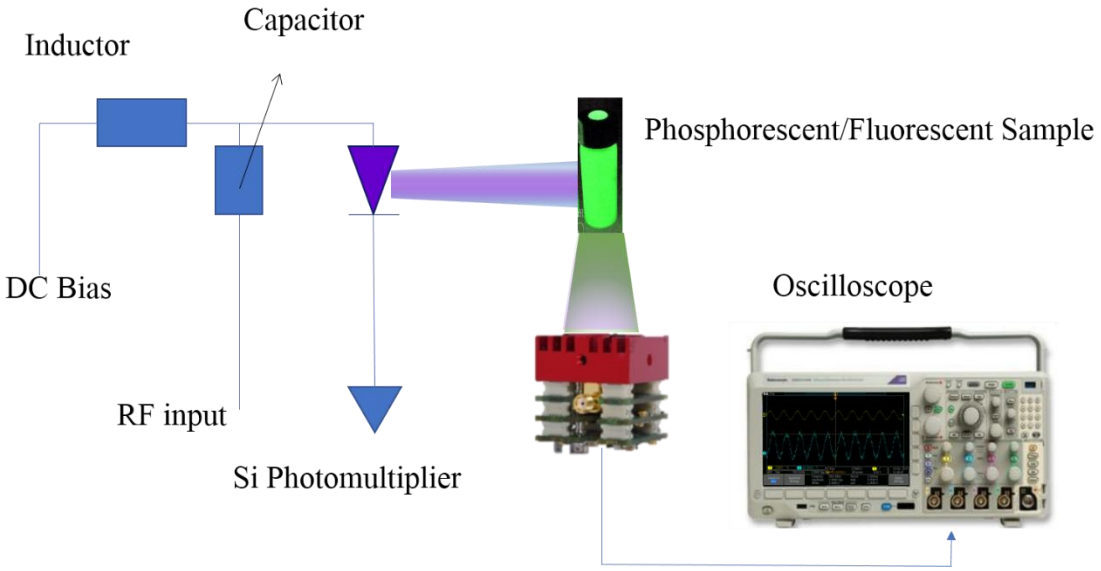

Figure 4.2: Demonstration of non-line of sight (NLOS) optical communication system.

A typical non-line of sight (NLOS) communication system is shown in Figure 4. 2. A high power Lumex 405 nm LED was modulated using Thor Labs LDC500 Laser Diode Controller which is basically a bias-tee (consists of the addition of signals from an ideal inductor which allows DC bias to pass blocking any RF signal and an ideal capacitor at which vice-versa happens). A sinusoidal modulation of 0. 5 MHz with amplitude 0. 9 V was fed to the LED from the AFG output of Tektronix MDO3024 200 MHz oscilloscope (figure 4. 3a). The modulated light was detected using SensL S/N 00558 SPMMini silicon photomultiplier module (SPM) of area $1mm^2$ and visualized using Tektronix MDO3024 200 MHz Oscilloscope with a sampling rate of 2. 5 GSa/s. The SPM has a built-in trans-impedance amplifier which converts and amplifies the photocurrent to photovoltage. The time series data in the oscilloscope was captured using an AC coupling of 1MΩ. Figures 4.3b and 4.3c show the modulated light detected in the presence of an empty vial and in the presence of a vial containing the phosphorescent material.

The magnitude of photon fluctuations present in a light source is proportional to the number of photons emitted per unit time. The presence of phosphor enhances the fluctuations in the light signal, resulting in the increase of the light signal's noise floor. Thus, for an appropriate distance between the light source and the detector, the phosphorescent noise can make up a sizable fraction of the modulation amplitude of the original LED light source leading to very low signal to noise ratio of data transfer.

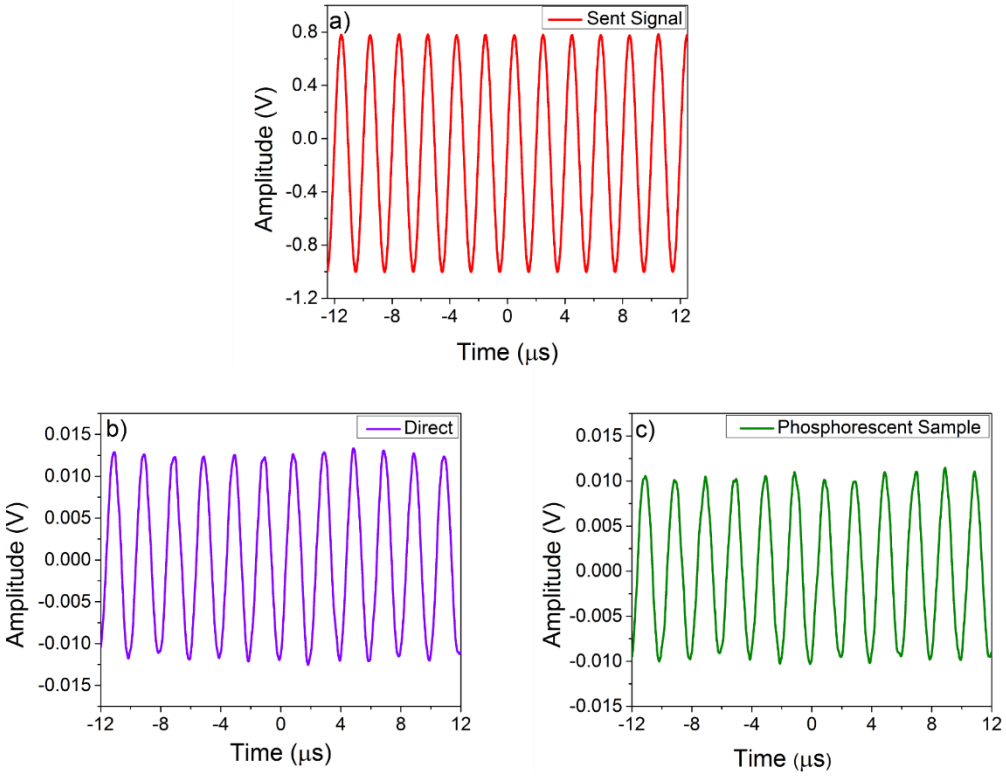

Figure 4.3: (a) Input waveform fed to the LED. Modulation Signal measured across the Silicon Photomultiplier Module for (b) direct (c) in the presence of a phosphor.

4.5 Sources of Noise

- Radiated electric and magnetic fields are the most common means of noise coupling. All circuit elements whenever charges move through them radiate electromagnetic waves. In addition, noise from external sources which include AC power lines, wireless communication waves from radios TV stations, wi-fi and Bluetooth signals can couple into electric circuits through conducting wires. For example, peaks at 50 Hz and its harmonics are due to the power line and a peak at 2. 4 GHz corresponds to Wi-fi and Bluetooth operation.
- Multiple paths to ground currents in a system give rise to ground loops. Several paths of conduction in instruments are arranged to regulate current flows and all paths are connected to common ground through a low impedance. This prevents the internal system to be at a floating potential between the AC supply potential and the earth ground. These multiple paths form a loop and can pick up stray signals by electromagnetic induction. The ground loop also results in an unwanted current through a conductor connecting two points

which are generally supposed to be at the same potential but are actually at different potentials.

- If the dielectric material inside the cable is not in contact with the cable conductors a charge can be produced on the dielectric which acts as noise voltage. This is termed as triboelectric effect and usually caused by mechanical bending of the cable or if the cable is left hanging without any support.
- There are always stray magnetic fields in the laboratory due to power wiring and other circuits with high current. If a wire is then allowed to move through this field a noise voltage gets induced in the wire. So, the motion of conductors has to be limited as much as possible. This problem is especially troublesome in a vibrational environment.

The interference of environmental electromagnetic noise sources can be diminished enormously by using shielded metal enclosure. This enclosure is called as Faraday cage. The setup is made of 2 mm thick aluminum and is cubical in shape. The inside of the Faraday cage was painted black to reduce the noise originating because of the reflections from the walls of the enclosure. The ground loop problem was avoided by shorting the Faraday cage with the ground of the digital storage oscilloscope (DSO).

4.6 Measurement of Photon Number Fluctuations

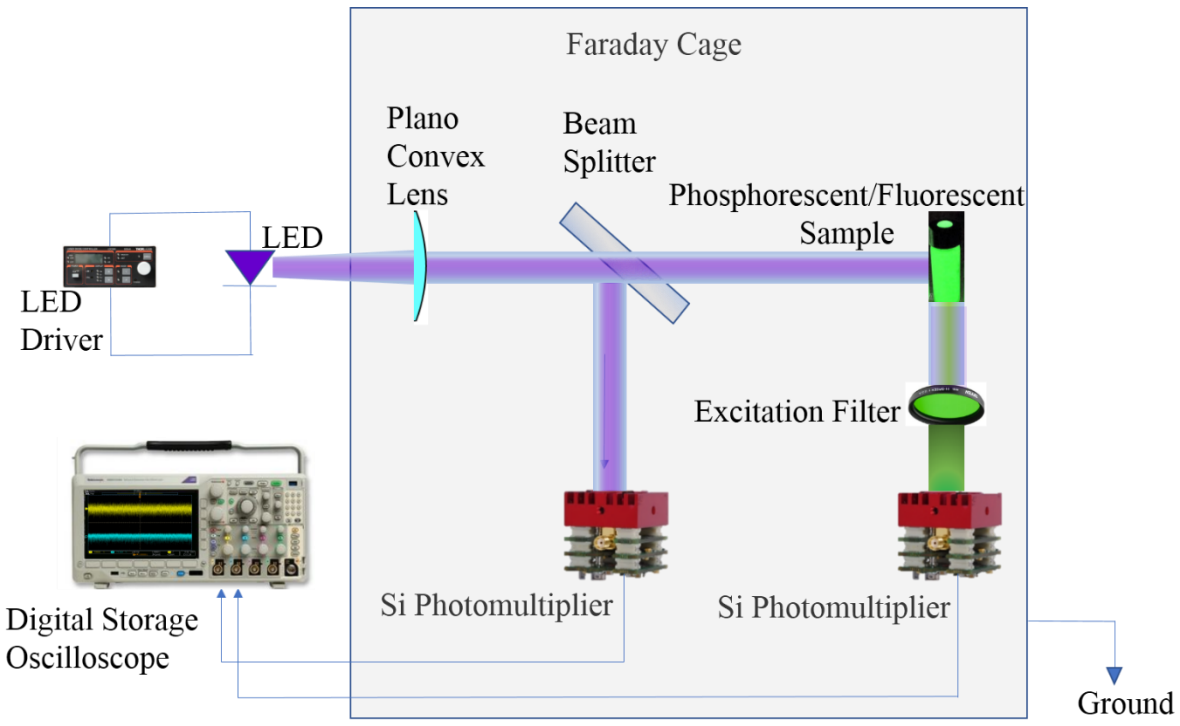

Figure 4.4: Schematic for measuring the photon number fluctuations from phosphorescent or fluorescent sample

The schematic for measuring the photon number fluctuations coming from the LED, phosphorescent and fluorescent sample is shown in figure 4. 4. A high power Lumex 405 nm LED was powered using a Thor Labs LDC 500 Laser Diode driver. The light from the LED was collimated using a plano-convex lens. The collimated light was then passed through a beam-splitter. The fluctuations in the light intensity reflected from the beamsplitter were detected using SensL S/N 00558 SPMMini Silicon photomultiplier module (SPM). The transmitted light was used to excite the phosphorescent or fluorescent sample. The fluctuations in the light intensity levels from the sample were captured using another SensL S/N 00638 SPMMini Silicon Photomultiplier Module (SPM). The time series data from both the Silicon Photomultiplier Modules was captured simultaneously using AC 1MΩ termination of Tektronix MDO3024 200 MHz Oscilloscope at a sampling rate of 100kSa/s for a 10s window. The whole setup was isolated from the environment using a grounded faraday cage to minimize acquiring of any spurious data. The captured time series data was transferred to a computer and the post processing of the data was done using MATLAB.

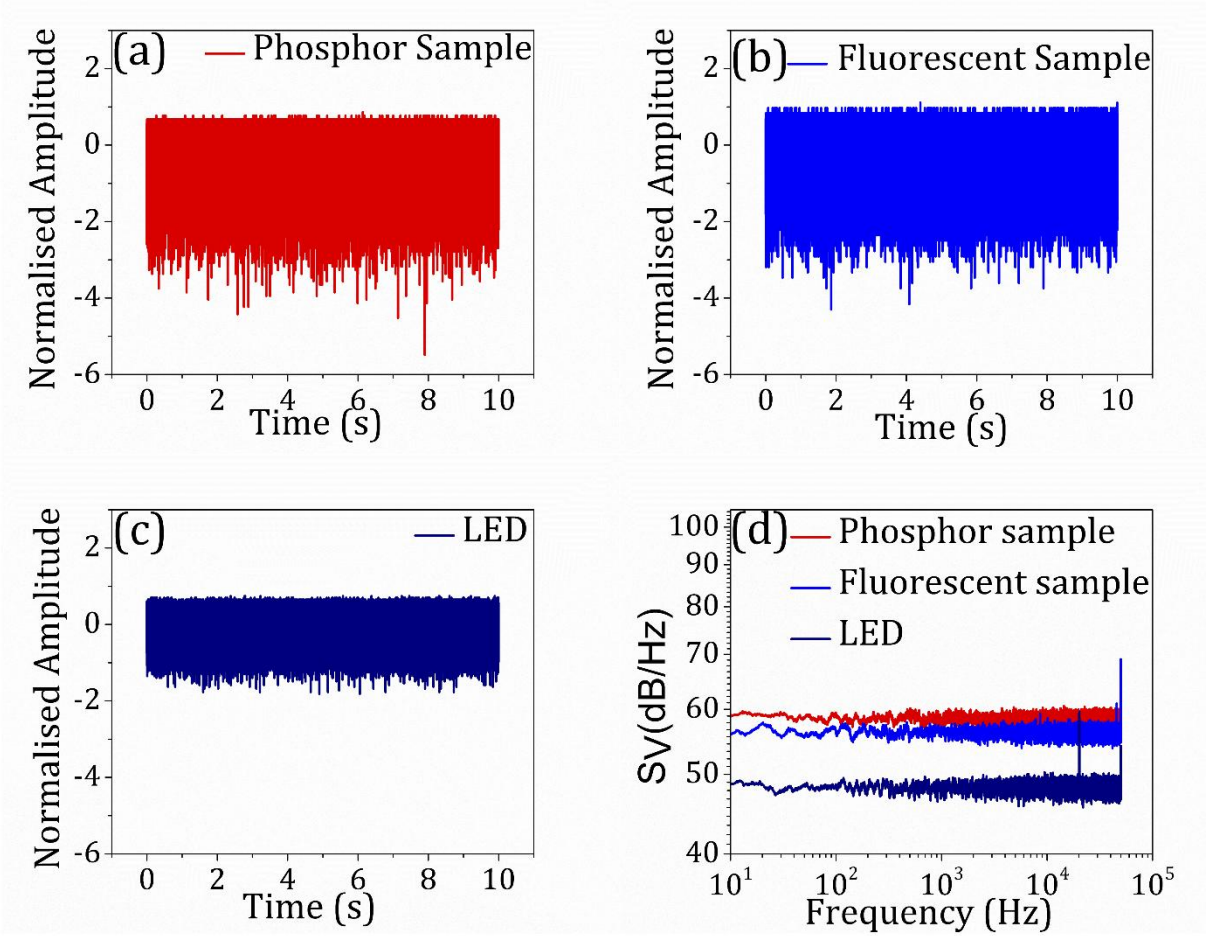

Figure 4.5: Noise measurement due to the presence of phosphor in an optical communication system. The fluctuations coming due to the phosphor were captured using SensL S/N 00638

SPMMini SPM and visualized in Tektronix MDO3024 200MHz oscilloscope using an AC coupling of 1 MΩ. The total time of capture of the data was 10s. Photon number fluctuation from the (a) phosphorescent sample (b) fluorescent sample. (c) LED (d) Power Spectral Density (S_V) plots for the time series data.

The $V(t)$ obtained for various samples were then normalized with respect to their dc photovoltage produced to keep the mean number of photons coming from different samples same. Upon comparing the recordings of $V(t)$ for different optical contributions, the importance of surface elements on the wall become evident. Figures 4.5a, 4.5b and 4.5c show the comparative time series data for the dark, phosphorescent and the fluorescent sample. The power spectral density, S_V was calculated from the time series data using the formula

$$S_V = \frac{1}{2T}\left|\int_{-T}^{T} V(t)e^{-2\pi ift}dt\right|^2 \qquad (4\text{-}8)$$

where T is the duration of the the capture of the time series data.

It is seen from Fig 2d that the magnitude of photon number fluctuation is independent of frequency and it is highest for the phosphorescent sample followed by the fluorescent sample and the LED for the same intensity of excitation of the LED.

Cross-Correlation Analysis

The cross-correlation function is defined as [15]

$$G_{12}(\tau) = \frac{c_{12}(\tau)}{\sqrt{c_{11}(0).c_{22}(0)}} \qquad (4\text{-}9)$$

where $c_{mn}(\tau)$ is the covariance between the two signals which is defined as

$$c_{mn}(\tau) = < v_m(t+\tau).v_n(t) > \qquad (4\text{-}10)$$

Here τ is the time lag between the time series data generated by the two SiPM – one recording the LED fluctuations and the other recording the fluctuations coming from the phosphorescent or the fluorescent sample.

Figure 4. 6 shows the variation of cross-correlation function with a time lag between the two detectors. There was no observed cross-correlation between the two detectors in the dark (Figure 4.6a) which justifies that the correlation is contributed mainly from the photons incident on the photomultiplier module. A sharp correlation was observed in the vicinity of $\tau = 0$ when the cross-correlation function was calculated for the fluctuations between the LED and the fluorescent

sample (Figure 4.6b) and when both the detectors received the same LED signal (Figure 4.6c). However, there was a very weak cross-correlation observed between the phosphor and the LED signal (Figure 4d).

The presence of the sharp correlation between the LED and fluorescent sample can be understood as follows:

The LED driver circuit injects electrons into the LED with fluctuations that follow a Poissonian distribution. These fluctuations from the LED driver get incorporated in the LED as the recombination mechanism of the LED is a stochastic process. Since the intensity of light used in the experiment is high (>10 $\mu W/cm^2$) , the number of photons emitted are large, thus, the noise distribution followed by these photons is of Gaussian nature.

After emission from the LED, the photons pass through a plano-convex lens and retain their Gaussian distribution. The beam splitter binomially selects the incident photons into transmitted and reflected beam. Thus, the Gaussian distribution of the LED photons is retained for both the reflected and transmitted beams which then falls on the phosphorescent or fluorescent sample.

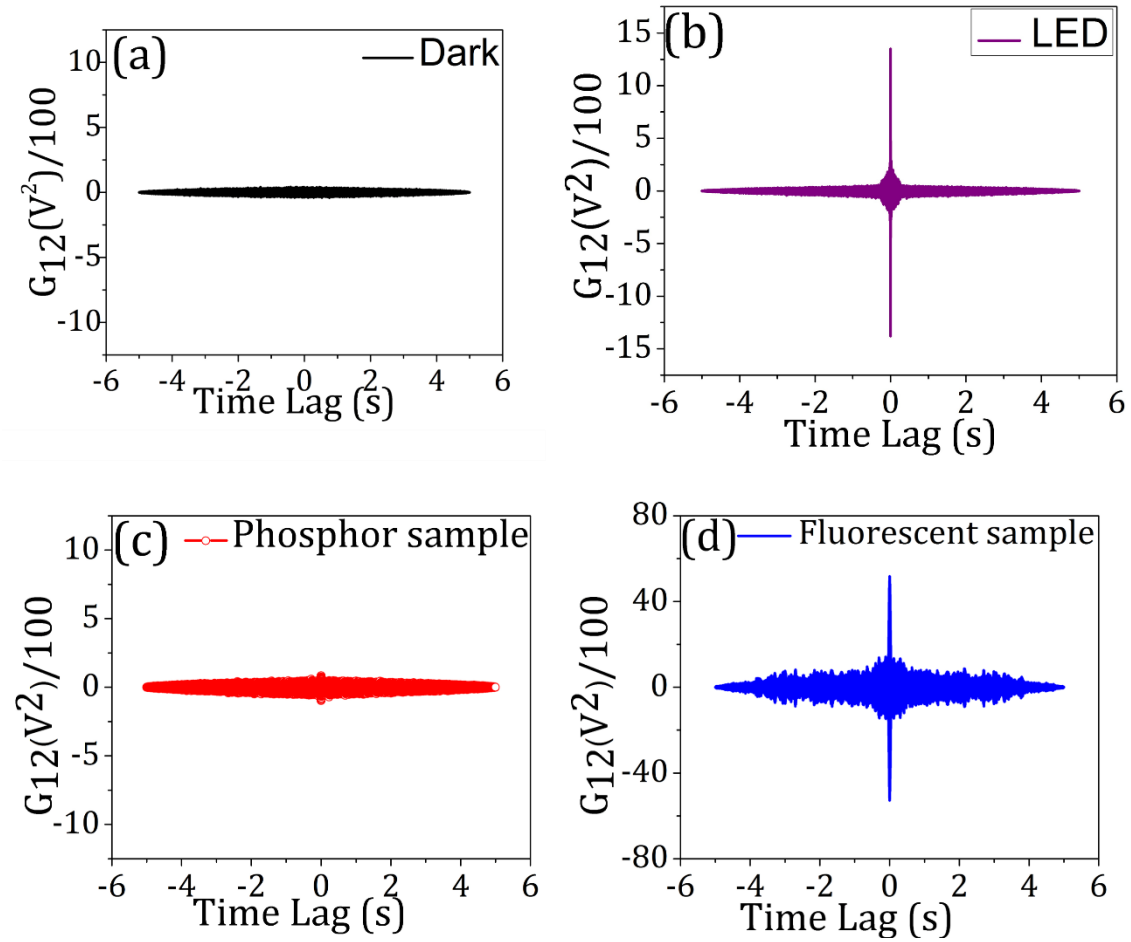

Figure 4. 6: Cross-Correlation Analysis of the fluctuations recorded by the two Si Photomultiplier Modules (a) dark (b) LED signal captured by the two detectors (b) LED and Phosphorescent sample (c) LED and Fluorescent Sample

The lifetime of a fluorescent sample is of the order of nanoseconds, thus it retains the photon number distribution coming from the LED. This is because of the fact that, at a particular point in the fluorophore the excitation and de-excitation time interval is much lesser than the time interval between the arrival of two photons successively.

The presence of cross-correlation when the two detectors received the same LED signal is self-explanatory as the nature of photon number distribution is same for the transmitted and the reflected light from the beam-splitter.

However, this is not the case for the phosphorescent sample where the presence of a metastable triplet state inhibits the above process to happen. Thus, the nature of the Gaussian distribution changes and hence we see a high correlation for a fluorescent sample than that for a phosphorescent sample. This proves the fact that the phosphorescent sample has the ability to

change the photon number distribution and can be used to scramble a modulated signal coming from an LED.

4.7 Modulation Of Phosphorescent Light to transfer data

An interesting application has uncovered during the course of our studies on the emission from the Strontium Aluminate phosphor coating which has exceptionally high lifetimes (glow in the dark paint). VLC can be achieved by switching off the conventional LEDs/laser, for a sustained duration. The remnant light from the phosphor paint can be tapped in as the photon source and acousto-optic modulation technique or bare mechanical choppers can be utilized for data transmission. Figure 4. 7 shows the transmission of phosphor modulated data using a mechanical chopper and a lock-in amplifier.

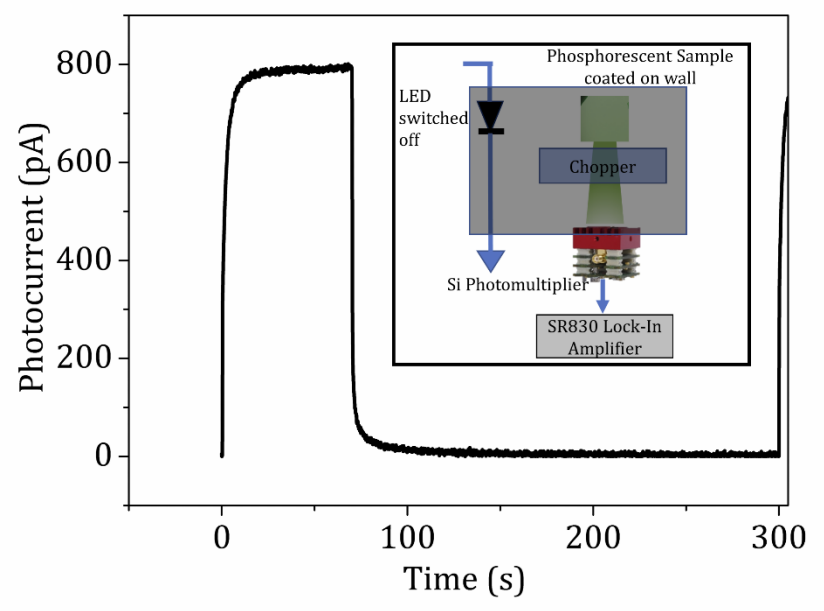

Figure 4. 7: Phosphor modulated at 3 kHz using a mechanical chopper and the photocurrent measured through SR830 Lock-in amplifier. The pulse corresponds to the excitation of the phosphor using a 405 nm LED. The inset shows the experimental schematic.

4.8 Conclusion

Our results indicate the utility of fluorescent and phosphorescent coatings to tailor and modify signal detection attributes in a VLC protocol. The possibility of tuning the signal to noise levels as a function of the spatial coordinates can be utilized to design smart environments where signal access can be controlled and restricted. Conversely, the signal analysis can also be utilized to provide dynamic information about the environment. We also demonstrate the feasibility of VLC

in dark conditions after the primary LEDs are switched off, which relies upon the emission persisting for a sufficiently long duration, and can also lead to novel applications.

4.9 References

1 Zhao, Y. & Vongkulbhisal, J. Design of visible light communication receiver for on-off keying modulation by adaptive minimum-voltage cancelation. *Engineering Journal* **17**, 125-130 (2013).

2 Chung, Y. H. & Oh, S. -b. in *Intelligent Signal Processing and Communications Systems (ISPACS), 2013 International Symposium on.* 749-752 (IEEE).

3 Yin, S. & Gnawali, O. Towards Embedded Visible Light Communication Robust to Dynamic Ambient Light.

4 Sajjad, M. T. *et al.* Fluorescent Red-Emitting BODIPY Oligofluorene Star-Shaped Molecules as a Color Converter Material for Visible Light Communications. *Advanced optical materials* **3**, 536-540 (2015).

5 Chun, H. *et al.* Visible Light Communication Using a Blue GaN $\ mu $ LED and Fluorescent Polymer Color Converter. *IEEE Photonics Technology Letters* **26**, 2035-2038 (2014).

6 Sajjad, M. T. *et al.* Novel fast color-converter for visible light communication using a blend of conjugated polymers. *ACS Photonics* **2**, 194-199 (2015).

7 Santos, J. *et al.* in *Photonics Conference (IPC), 2016 IEEE.* 396-397 (IEEE).

8 Chow, C. , Yeh, C. , Liu, Y. & Huang, P. Mitigation of optical background noise in light-emitting diode (LED) optical wireless communication systems. *IEEE photonics Journal* **5**, 7900307-7900307 (2013).

9 Sindhubala, K. & Vijayalakshmi, B. Review On Impact Of Ambient Light Noise Sources And Applications In Optical Wireless Communication Using LED. *International Journal of Applied Engineering Research* **10**, 31115-31130 (2015).

10 Liu, Y. , Yeh, C. , Wang, Y. & Chow, C. in *OptoElectronics and Communications Conference and Photonics in Switching.* TuPR_10 (Optical Society of America).

11 Hakim, N. , Saleh, B. & Teich, M. Generalized excess noise factor for avalanche photodiodes of arbitrary structure. *IEEE Transactions on Electron Devices* **37**, 599-610 (1990).

12 Eckert, P. , Schultz-Coulon, H. -C. , Shen, W. , Stamen, R. & Tadday, A. Characterisation studies of silicon photomultipliers. *Nuclear Instruments and Methods in Physics Research Section A: Accelerators, Spectrometers, Detectors and Associated Equipment* **620**, 217-226 (2010).

13 Rech, I. *et al.* Optical crosstalk in single photon avalanche diode arrays: a new complete model. *Optics express* **16**, 8381-8394 (2008).

14 Bachor, H. -A. , Rottengatter, P. & Savage, C. Correlation effects in light sources with high quantum efficiency. *Applied Physics B: Lasers and Optics* **55**, 258-264 (1992).

15 Endo, T. , Morimoto, E. , Hirayoshi, Y. & Toyoshima, K. Anticorrelated noise from parallely connected light emitting diodes. *Journal of the Physical Society of Japan* **67**, 3082-3085 (1998).

CHAPTER 4

CHAPTER 4

CHAPTER 5

SUMMARY AND FUTURE DIRECTIONS

Free space communication via Li-Fi further utilizes off-the-shelf light-emitting diodes (LEDs) and detectors to realize fully networked wireless systems. LEDs are natural beamformers which enable local containment of Li-Fi signals. The primary goal of VLC is to use the existing LED lighting technology to be also used for communication. Generally, the LEDs used for lighting in homes and offices are composed of GaN (having electroluminescence emission from 405 nm to 450 nm) coupled to an yellow phosphor to give rise to a spectrum that is composed of white light. However, this yellow phosphor component has a lifetime in the order of milliseconds. This reduces the switching speed of the white LEDs immensely, making them not viable for communication. Thus there are two ways by which this fundamental problem in VLC can be solved. The first goal is to replace the existing phosphor used in white LEDs to color converters which has very less lifetime. The second way is to have a photodiode that has a reduced overlap of absorbance with the phosphor spectra. Organic semiconductors with their vast advantages such as band gap tunability, high absorption coefficient, easy fabrication, etc. are perfect for this application. Polyfluorenes are donors with a very high absorption coefficient in the blue region and they have a very narrow bandwidth of absorbance. Thus. with an appropriate acceptor they can be used to fabricate photodiodes that has very less overlap with the yellow phosphor.

Chapter 2 deals with a bulk heterojunction (BHJ) based organic photodiode consisting of poly(9,9-dioctylfluorenyl-2,7-diyl) (PFO) as the donor and [6-6]phenyl-C61-butyric acid methylester (PCBM) as the acceptor. The photodiode exhibits a significant high responsivity from 400 to 500 nm with full width at half maxima (FWHM) of ~140 nm which ascertains the fact that this device can be tuned as a very narrowband blue filter-less photodiode. The FWHM can be tuned by changing the thickness of the active layer. However, this will also have an effect on the speed of response of the photodiode. Therefore, the thickness has to be optimized for it to be used as a detector in visible light communication. The temporal bandwidth and the FWHM of the responsivity spectra as a function of the device of the device is needed to be studied further. Also, the responsivity

of the device has a small overlap with the emission spectra of the phosphor i.e., it filters out the background yellow phosphor emission massively to enhance the bandwidth of communication. Thus studies with the off the shelf white LEDs with this device is needed to be done.

To enhance the responsivity of the detector in the near infra-red (NIR) region, a NIR dye was added to this binary blend which is discussed in Chapter 3. The photodiode showed higher responsivity of >10 mA/W and temporal response > 0.8 MHz. Thus this photodiode can be used in CSK type modulation where it can be used to detect data from two LEDs – one having emission in the blue region and one having emission in NIR region thus increasing the bandwidth of communication.

Chapter 4 deals with the influence of various coatings on the wall (both phosphorescent and fluorescent) in the non-line of sight visible light communication. The enclosure boundary normally is treated as a classical light diffuser which merely scatters and attenuates the signal. The use of various photo-luminescent coatings on walls acts as active noise sources which distort the signal and alter the communication characteristics. The possibility of tuning the signal to noise levels by these emitters as a function of the spatial coordinates can be utilized to design smart environments where signal access can be controlled and restricted. Conversely, the signal analysis can also be utilized to provide dynamic information about the environment. The chapter also deals with the feasibility of VLC in dark conditions after the primary LEDs are switched off, which depends upon the emission persisting for a sufficiently long duration, and can also lead to novel applications.